Earth Surface Dynamics Discussions (esurf-2017-50)

Bumps in river profiles: the good, the bad, and the ugly
Wolfgang Schwanghart and Dirk Scherler

Final response to comments by reviewers

Reply: We thank both reviewers for their helpful and constructive comments. Please find below our point-by-point replies to each of their comments. We have implemented the suggestions in the manuscript and show these changes as indented text together with our replies.

Reviewer 1:

In this paper, the authors propose an innovative method to smoothen the longitudinal profiles derived from digital elevation models (DEMs) using a quantile-based statistics, called constrained regularized smoothing (CRS). The work is well presented, and the manuscript is ready to follow with an appropriate number of figures in good quality. The authors demonstrate extensive analysis on the proposed method using various kinds of global DEMs to find the pros and cons of the DEMs themselves, as well as to test the applicability of the smoothing method (CRS) to the noisy, DEM-derived channel profiles of both mainstream and tributaries. I believe this work is worth being published in the journal Earth Surface Dynamics, subject to some minor corrections.

We thank Reviewer 1 for his/her constructive assessment of our work.

{General comments}

CRS-derived gradient:

I think the paper would be strengthened if some additional demonstrations are provided. The authors show the nicely smoothed channel profiles, but do not provide the derivatives of the along-stream elevation (slope gradients). In the discussion, the authors state that "CRS-smoothing of river profiles can decrease differences to actual river elevations and gradients" (P10 L4), but the along-stream gradients after the CRS processing are not really provided. Furthermore, they mention that the CRS method will be useful for the analyses of knickzones and hydrolodynamics that often use stream gradient, and the representation of gradients can be highly of interest for many researchers working on fluvial (and other) processes. It can be more clearly demonstrated if they could show some examples from their own datasets – even just a visual representation (not a strict statistics) would help readers to understand the advantage of the CRS method in calculating the derivatives of elevation. I would, therefore, recommend adding a figure that shows not only the elevation profiles but also the slope (and curvature, if applicable) derived from the original and CRS-applied datasets.

We thank Reviewer 1 for this suggestion. In the revised manuscript, we provide additional visualizations that allow readers to interpret the results from the CRS algorithm. Derivatives of longitudinal river profiles (e.g. along-river gradients) were also addressed by Reviewer 2 and we detail some findings below that we will include in the revised manuscript.

Title:

The title sounds attractive, but not fully informative. Particularly, "the good, the bad, and the ugly" is vague. It would be better to include the key terms (such as global DEMs, quantile carving, and/or constrained regularized smoothing).

We changed the title to: Bumps in river profiles: uncertainty assessment and smoothing using quantile regression techniques

Objectives:

At the beginning of "4. Methods and data", the authors provide an explicit description of the goals of this study (P6 L22-L24), but these were not so clearly shown in the Introduction section (P2 L5-8). Please rewrite the objectives more clearly in Introduction.

We have rewritten the aims and objectives in the introduction:

> ***The objective of this study is to characterize and quantify the uncertainties of elevation values in longitudinal river profiles derived from near-globally and publicly available DEMs including the new TanDEM-X DEM. To attain this goal, we devise new algorithms (quantile carving and constrained regularized smoothing) that use non-parametric quantile regression for assessing uncertainties and smoothing of river profiles. Using LiDAR DEMs as benchmark data and our new algorithms, we study how longitudinal river profiles derived from globally available DEMs (Table 1) are affected by errors and how these errors depend on the topographic setting. Moreover, we examine the best choice of parameter values for our algorithms to guide their application. Our algorithms will aid the visual interpretation and automated analysis of longitudinal river profiles and has additional applications in hydrodynamic modelling.***

{Specific comments}

P7 L4 "ellipsoidal heights (WGS84)" Which geoid was applied for each dataset (or the same for all)?

Please see subsequent comment below.

P7 L5 "resampled... resolution" To what resolution? How? (nearest neighbor?)

We rewrote this sentence to clarify the geodetic height datum and the type of resolution:

> ***"We used the reference ellipsoid defined by the world geodetic system WGS 84 as basis for all DEMs and resampled them to the same spatial extent and 30 m resolution using bilinear interpolation".***

P10 L16 In this section the authors seem to discuss some sorts of errors. I do not figure out why they mention each error type as "good", "bad", and "ugly". I am sorry if I am missing some, but it would be better clarified – the differences of goodness, badness, and ugliness of each error.

We rewrote this section and avoided the terms good, bad and ugly.

River profiles are derived from measurements that give rise to errors of different types: random and systematic components, as well as artifacts (Reuter et al., 2009). We have shown that the CRS algorithm can efficiently handle random errors and may reduce offsets that arise from systematic or artefactual deviations between actual river profiles and those derived from DEMs, thus improving an overall representation of longitudinal river elevations and gradients. Caution, however, must be taken with autocorrelated errors that we have not addressed here although they may significantly affect river profiles. Autocorrelation entails that if the true elevation at some location is overestimated in the DEM, then the elevation at a nearby pixel will likely also be overestimated (Temme et al., 2009). Autocorrelated errors have important consequences for the choice of smoothing parameters. In the case of short-range dependence, profiles may not be affected severely if a sufficiently large smoothness parameter is chosen. Long-range dependence, however, is neither easy to detect nor their structures simply removed by non-parametric regression. For example, it is difficult to ascribe the stepped patterns in Fig 3b to actual riffle-pool sequences or to artefacts that should be smoothed (Fig. 3c). Although approaches to nonparametric regression exist that are able to cope with autocorrelated errors (Opsomer et al., 2001), their implementation and assessment were, however, beyond the scope of this study.

P11 L6-7 Although I did not find any detailed descriptions of the smoothing method in Bricker et al. (2017), if the CRS algorithm (or a similar one) has already been presented in the previously published article, I think it should be explicitly shown prior to the methodological descriptions in this paper.

The study of Bricker et al. (2017) used a previous version of the algorithm and was applied to a single reach and not an entire river network and not tested in detail. We thus refrained from a detailed mathematical description of the algorithm in that paper. Nevertheless, we changed the wording in this sentence:

In a recent study on flash flood warning and hazard assessment in the Nepal Himalaya, a preliminary version of the CRS algorithm provided an important preprocessing step to improve the accuracy of estimating flow depth, flow speed, and flood wave arrival times (Bricker et al. 2017).

P11 L17 "other variables" such as...??

We added examples as requested:

Finally, the CRS algorithm is not restricted to elevation profiles, but can also be applied to other variables measured or calculated along river profiles such as steepness (Ksn) or curvatures both of which are usually prone to even larger uncertainties.

Table 4 It would be better to show that the values of RMSE are the deviations from the ALS data in this caption (not only in the main text).

Yes, we have added this information to the caption of Table 4:

The root mean squared error (RMSE) is calculated from the deviations from the LiDAR data.

Fig. 8 Please explain "Topographic shielding" in details. Does this corresponds to the "hillslope gradients adjacent to river within 1000 m distance"?

According to Codilean (2006), topographic shielding refers to the proportion of the incoming cosmic radiation that is shielded by the surrounding topography. It is used in cosmogenic nuclide dating to correct for decreased production rates in steep terrain. We accidently plotted topographic shielding instead of hillslope gradient in Fig. 8 of the manuscript, and we have now changed it to hillslope gradient within 1000 m distance from the stream network. The patterns, however, are similar as both measures are highly correlated and thus the changes do not affect our conclusions.

{Technical corrections}

P6 L13 The details of the place name appears later, but here please provide, at least, the region name "(San Gabriel Mountains, USA)" where "Big Tujunga catchment" locates.

Done

P13 L11 "Eq. (11)" does not seem to appear elsewhere in the manuscript.

Eq 11 has been changed to Eq A6.

P14 L11-12 The numbering of the equation may be A12.

Done

References:

Codilean, A.T. (2006): Calculation of the cosmogenic nuclide production topgrahic shielding scaling factor for large areas using DEMs. Earth Surface Processes and Landforms, 31, 785-794.

Reviewer 2 (Fiona Clubb):

This manuscript presents a new method for smoothing river long profiles based on a quantile-carving approach, which the authors then use to examine errors in elevation values extracted from different globally available DEMs. The paper is interesting and well-written, and provides useful insight into the applicability of different global DEMs for fluvial profile analysis as well as presenting a novel algorithm which has potential to be used in many studies. I think that the paper is suitable for publication in Earth Surface Dynamics following some minor corrections, which I have detailed below. Some general points:

- In many studies analysing river profiles, other metrics, such as channel gradient and drainage area, are used along with elevation to examine channel response to changes to external forcings such as climate or tectonics. It would be useful to include some analysis of how these metrics vary between the different DEM datasets, or with and without the CRS smoothing algorithm, as these are key datasets that will be needed in channel profile analysis by any users of the code. I suggest expanding the analysis (either by including a figure or another table) to include statistics of the channel gradients.
  We agree with Reviewer 2 that addressing along-river gradients more explicitly would be

useful. We have done additional analysis on gradients that we detail further below in this reply and that are included in the revised version of the manuscript.

- The calibration of the parameters K and τ clearly has a large impact on the elevation values extracted from the profiles (e.g. Fig 3). Although the authors discuss the fact that these parameters can affect the elevation values, it would be useful to include some more guidance on how these parameters can be set by the user to avoid over- or under-smoothing their channel profiles. This has been done for the K parameter in Section 6.2, but it would be useful to also include information on the sensitivity of the method to τ.
  Profiles for different values of tau are shown in Fig. 3. Yet, the reviewer is right that we have not explicitly addressed the sensitivity of the smoothed profiles to changes in tau, largely because tau does not primarily affect the form of the profile but rather vertically shifts the profile. However, for very large (>0.99) or low (<0.01) values of tau, the algorithm shows some misfits to the data in particular if there are only few data points in the profile. We interpret this behavior to be related to difficulties of deriving quantiles for a limited amount of data points (see our sensitivity test below). We have addressed this issue in the revised version of the manuscript and included a sensitivity analysis.

- I wonder if there is potential to include a spatially variable K parameter along the profile based on the distribution of local relief (e.g. where the K parameter is calculated directly from the relief of the surrounding landscape, rather than having to be set by the user)? This could be useful in areas like the Nepal site where the topography varies dramatically along profile. I'm not suggesting doing this for the paper, but it may be useful to include as a potential avenue of development for the method.
  We thank Reviewer 2 for this suggestion. In fact, we mention this possibility in the last paragraph of the discussion. We do not plan to include spatially variable K or tau in a revised version. This would require deriving a statistical model between e.g. hillslope gradients and K which is beyond the scope of this paper. However, we consider implementing such option in a newer version of TopoToolbox in the future.

Specific comments

Page 1, Line 23: river profiles may also reflect signals of base level and sediment transport processes.

We have changed the sentence accordingly:

The geometry of a river and specifically its longitudinal profile, reflect the climatic and tectonic forcing, variations in base level and sediment transport processes as well as differences in bedrock erodibility.

Page 2, Line 3: clarify here that bumps in river profiles may also be from real signals of climatic/tectonic perturbations in the profile.

We have changed the second half of the paragraph according to the suggested change:

Structures such as bridges, culverts and reservoirs affect longitudinal river profiles derived from DEMs in ways that can either hide features present in reality or introduce patterns

that do not represent the actual course of the profile (Schwanghart et al., 2013). Deviations from graded river profiles may reflect signals of climatic or tectonic perturbations, but often they relate to errors and artifacts that generate bumpy river profiles and thus introduce uncertainties that may compromise the interpretation of longitudinal river profiles (Hayakawa and Oguchi, 2006; Wobus et al., 2006).

Introduction: traditional methods of analysing river profiles to extract climatic/tectonic signals generally use slope and area as well as the elevation of the river profiles. It would be useful to mention these metrics in the introduction and how they relate to the extraction of the elevation values.

Yes, we mentioned these metrics in the revised the manuscript (see next comment).

I think the introduction could be expanded to review some of the advantages of fluvial profile analysis and to include some more literature on how these methods have been applied in the past. At the moment I think this is slightly glossed over, and it would be good to emphasise this to show the value of the authors' new method for the geomorphology community.

We have tried to keep the introduction as short as possible and instead chose for a more detailed account of DEM errors and their effects on river profile analysis in the second section of the manuscript. However, in order to make the paper more accessible to other readers, we expanded our discussion of the literature on fluvial profile analysis in the first paragraph of the introduction.

Rivers play a dominant role in the topographic evolution of the Earth surface, and possibly other planetary bodies (Hack, 1957; Howard, 1998; Whipple et al., 2013). They transfer sediment from mountains to depositional basins, set the base level for hillslopes, and convey tectonic and climatic signals across landscapes. The geometry of a river and specifically its longitudinal profile, reflect the climatic and tectonic forcing, variations in base level and sediment transport processes as well as differences in bedrock erodibility. Gradients along rivers, for example, reflect spatial variations in uplift rates (Whipple et al., 2013; Mudd et al., 2014; Scherler et al., 2014) and indicate the extent of past glaciations (Brardinoni and Hassan, 2006). Moreover, they can act as predictors for the zones of erosion and sediment accumulation during extreme events (Devrani et al., 2015) and reflect the repeated impact of masswasting events (Korup, 2006). Longitudinal river profiles and metrics derived them (e.g., the normalized channel steepness metric k_{sn} (Wobus et al., 2006)) have become important tools for studying the topographic evolution of mountain belts and deciphering changes in climate and tectonics (Bishop et al., 2005).

Page 3, Line 32: I think it would be useful to expand upon these methods here and provide references for these approaches, since these are the benchmark algorithms which the authors are trying to improve upon with their method.

We added several references to these methods.

Page 4, Lines 2-5: Is this the running average approach demonstrated in Figure 1?

No, Fig. 1 shows a simple running average approach whereas Aiken and Brierley (2013) used a robust version of local regression using weighted linear least squares and a 1^{st}-degree polynomial

model. Our reference to Fig. 1 should illustrate that profiles may contain sections with downstream increasing elevations. We realized that this is ambiguous. We thus rewrote these sentences:

> ***Finally, even robust approaches that aim at reducing the influence of individual outliers on the smoothed curve (Aiken and Brierley, 2013) may yield profiles that contain sections with downstream increasing elevation that result from long sections where valley bottom elevations are overestimated. An example of how outliers may generate downstream increasing elevations in profiles smoothed by a running average is shown in Fig. 1c.***

Page 4, Line 9: It would be helpful for the authors to restate the aims and approach of the study here to emphasise to the reader how the method that they outline improves upon previous methods given the research needs stated in this paragraph.

We agree that it is a good idea to restate the aims after having defined the problems that we derive in the state-of-the-art section. In the revised version of the manuscript, we restate the aims of the study at the beginning of the methods section.

Figure 1: It would be good to highlight particular sections on the different profiles where the elevation increases downstream to make this clearer to the reader.

We changed Fig. 1 following this comment.

Page 4, Line 30: The authors state that the CRS method assumes local smoothness of the profile and spatial autocorrelation. I agree that a non-parameteric approach is very useful, as we don't have to assume that the channel is incision based on a specific model (e.g. stream power), but what is the justification for assuming that these should be local smoothness/spatial autocorrelation? We might expect this to be the case if the profile is in steady state and is nicely concave, but what about if the profile is transient? This will create local patches within the profile which are 'bumpy' or perhaps not spatially correlated. How easy is it for the method to differentiate between these and DEM artefacts?

Good point! The justification for assuming spatial autocorrelation or local smoothness is the First Law of Geography (also termed Tobler's law), which states that "near things are more related than distant things", an assumption that underlies all interpolation and smoothing techniques. Spatial autocorrelation is indeed vital for any kind of spatial analysis (De Smith et al., 2007) and should guide the value of a smoothing parameter together with the question and spatial scale underlying an analysis. In river profile analysis, our primary assumption is that of downstream decreasing elevations which justifies flood filling, carving and quantile carving. Local smoothness provides an additional assumption that is supported by the notion that river profiles usually do not exhibit the stepped profiles that appear in DEM-derived profiles, a notion that is supported by the analysis of better and higher resolution data in this study. Yet, Reviewer 2 is right in that she argues that transient river profiles may contain bumps or lack spatial autocorrelation. In fact, river profiles may have riffle-pool sequences or stationary knickpoints even if they are in steady state. Can CRS differentiate these real bumps from artefacts? No. CRS is not a classification algorithm. It smooths the profiles to remove scatter while accentuating the actual patterns in the data. However, quantile regression enables to derive uncertainty bounds which will support data interpretation and quantify DEM artefacts.

Page 6, Eq 4: How does the sensitivity of the method vary with grid resolution (4x)? From equation 4 it seems that the smoothing should increase as the resolution becomes coarser.

Good point. In fact, the squared spatial resolution (Δx) in Eq. 4 renders the degree of smoothing independent of the spatial resolution as it cancels out the squared distances in Eq. A4. Eq. 4 thus entails that a profile smoothed by the algorithm with a smoothing parameter K is insensitive to a linear transformation of the distance x.

Conversely, if we resample a given profile to a higher resolution, then a different value of K is required to obtain the same or at least similar smoothing results to those of the smoothed original profile. Here, the values of s (see Eq. 4) must be the same. For two profiles (A and B) with different spatial resolution Δx_A and Δx_B, and smoothing parameter K_A, the smoothing parameter K_B provides similar or same profiles if calculated by

$$K_B = (\Delta x_A / \Delta x_B)^2 K_A$$

We tested this relation using the following MATLAB script

```
%% Load data
DEM = GRIDobj('srtm_bigtujunga30m_utm11.tif');
FD = FLOWobj(DEM);
% Stream network A
SA  = STREAMobj(FD,'minarea',500000,'unit','map');
SA  = klargestconncomps(trunk(SA));
% Stream network B
DEMB = resample(DEM,15);
FD  = FLOWobj(DEMB);
SB  = STREAMobj(FD,'minarea',500000,'unit','map');
SB  = klargestconncomps(trunk(SB));

% Smooth
K_A = 5;
zsA  = crs(SA,DEM,'K',K_A,'split',false);
zsB = crs(SB,DEMB,'K',(DEM.cellsize./DEMB.cellsize)^2*K_A,'split',false);

% Plot
plotdz(SA,DEM,'color','b')
hold on
plotdz(SB,DEMB,'color','k')
plotdz(SA,zsA,'color','b','LineWidth',2)
plotdz(SB,zsB,'color','k','LineWidth',2)
hold off

legend('original profile A (30 m resolution)',...
       'profile B from resampled DEM (15 m)', ....
       'smoothed profile (30 m, K_A = 5)', ...
       'smoothed profile (15 m, K_B = (30/15)^2 K_A')
```

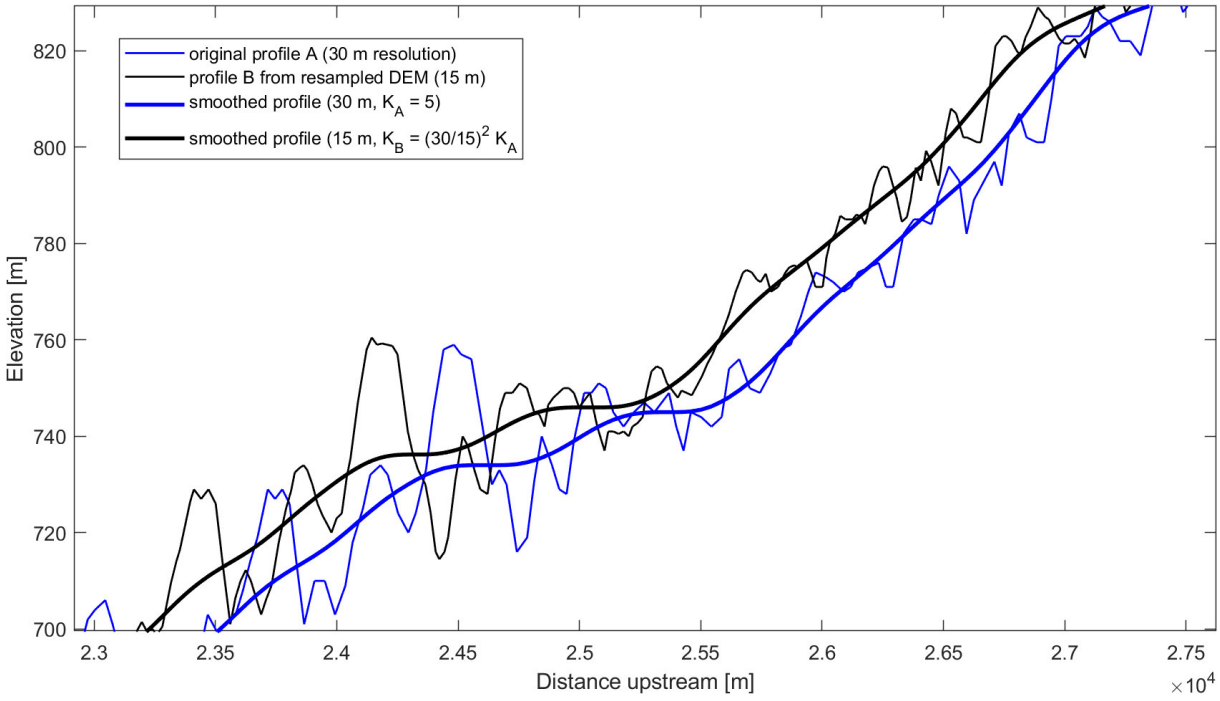

Fig. 1: Comparison of CRS-smoothed profiles of the Big Tujunga river derived from the original SRTM-1 (30 m resolution, A) and a resampled DEM (15 m, B). To obtain a similar smoothing result for B, K_B must be adjusted to take account for the differences in spatial resolution. The slight horizontal offset between the profiles is an artefact that arises from changed flow distances due to DEM resampling.

We added the following text together with the above Equation (as Eq. 5):

> ***"Larger values of the smoothing parameter K result in smoother profiles (Fig. 3). We include the squared spatial resolution into the equation so that any linear transformation (e.g. distance scaling) of the river profile does not affect the smoothing results. Yet, this entails that profiles with different spatial resolutions must be smoothed with different values of K to obtain the same or at least similar results. If two profiles A and B have different spatial resolutions Δx_A and Δx_B, then smoothing both profiles will return similar results if the smoothing parameter K_B is calculated from K_A by Eq. (5)."***

Fig 3: It looks like the smoothing parameter K and τ have a big effect on the final shape of the profile. How should the user choose appropriate values of these parameters? This is maybe explained later in the paper.

We have added a sensitivity analysis that illustrates the effect of variable K and tau on both elevation and gradients obtained from longitudinal river profiles. We added following figure to the manuscript to illustrate the sensitivity analysis and describe them in the methods, results and discussion.

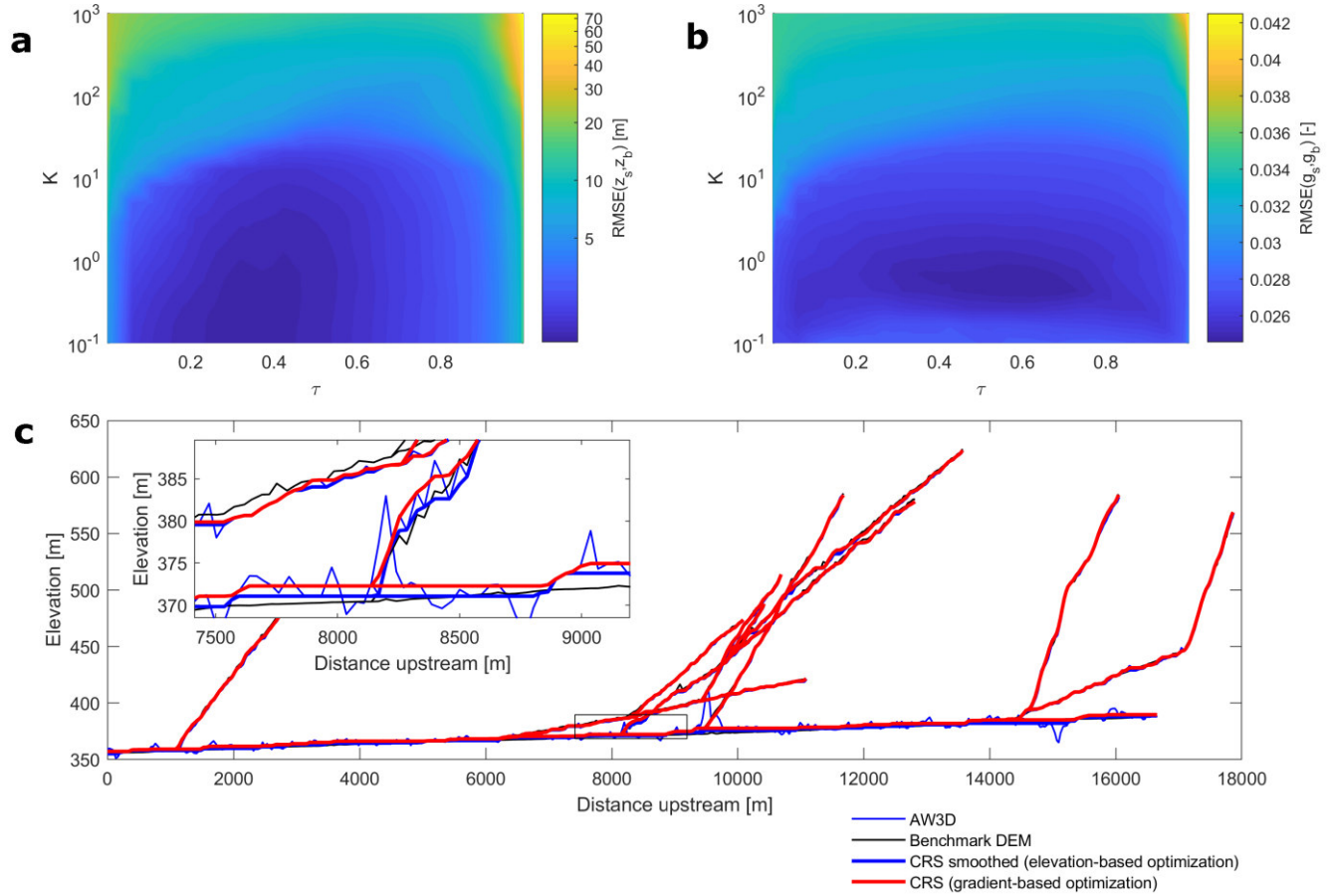

Fig. 2: Sensitivity analysis of the CRS algorithm and the smoothing parameter K and quantile tau for the Yakima catchment and the AW3D DEM. a) Sensitivity of the root mean squared error (RMSE) between smoothed elevations and elevations from the LiDAR derived benchmark profile. b) Sensitivity of the RMSE between gradients derived from the smoothed profiles and the benchmark profile. c) Profile of the Yakima and its tributaries and detail (see inset).

Table 1: It would be useful to include the vertical errors on each of the datasets used in the study.

We added the vertical errors to the footnotes in Table 1.

Page 7, Line 4 and throughout: Although the lidar DEMs are much higher resolution than the global datasets, it would still be useful to acknowledge/quantify the errors associated with these datasets. How were they gridded/filtered? What is the vertical error on the resulting DEMs? When was the lidar data flown compared to the global datasets (any temporal differences that could account for some of the error)?

The LiDAR DEMs used in this study have an elevation accuracy of 5-30 cm, ±1-sigma. The DEMs are bare-earth DEMs and their derivation using the software TerraScan is explained in the processing reports available on opentopgraphy.org. The Yakima data was acquired in 2008 and the Big Tujunga data obtained in 2007, which is later than the acquisition of the SRTM and overlaps or is prior to acquisition of the ALOS and ASTER data. We cannot exclude any temporal differences although we expect that these were minor and local. We added the following text:

> ***The LiDAR DEMs are bare-earth DEMs derived from point clouds (>3 points/m^2) and were downloaded from the OpenTopography facility (Table 1). Due to their decimeter to sub-decimeter accuracy, we consider the LiDAR data as our benchmark DEMs. The acquisition dates of the DEMs vary but we expect that temporal changes in the land surface are minor.***

Page 7, Lines 15-17: Would it be possible to vary the K parameter spatially, for example, correlated with relief/gradient? This could be useful for sites such as the Nepal one where there is a large difference in relief along the profile. May be beyond the scope of the paper for the moment, but it would be interesting to see if there was a correlation between the required smoothing parameter and the surrounding relief, so you could preferentially smooth the profile in areas more prone to errors.

Yes, it is possible to vary K spatially. As errors vary spatially as a function of hillslope gradients, it is a good idea to model K as a function of hillslope gradient. We mention this possibility in the last paragraph of the discussion. While we have not yet implemented optional spatially variable K in the software implemention of the crs algorithm, we may do so in the future.

Page 7, Lines 24-28 and Appendix B: I downloaded TopoToolbox and implemented the CRS smoothing method (which was easy to do!). It may be useful in the Appendix to include a link to a tutorial for using the CRS method, which I saw exists on the TopoToolbox wordpress. The authors have provided the tool crsapp for visual checking of the parameters, which is great, but it would be useful to provide a tutorial for use of this tool as well.

As mentioned by the reviewer, we have included the short tutorial on ksn values in our blog. There will certainly be more posts on this. Thus, we included a link to our blog (http://topotoolbox.wordpress.com) in the Appendix B.

Figure 5: Could you expand upon this caption to show what is being represented here? Is this the offset for every pixel in the river profile?

Yes, we have changed the caption:

> ***Fig. 5: Elevation offsets between different DEMs and benchmark LiDAR DEMs calculated for all river pixels for the Yakima and Big Tujunga dataset (see Fig. 4).***

Figure 7: It would be useful to see these data for the other two field sites as well as for the Nepal site, to show visually how the distribution of the residuals varies with relief.

We have changed Figure 7 to include the other sites as well (see below). Note that we also chose to logarithmically scale the x-axis which better illustrates the tails of the distributions.

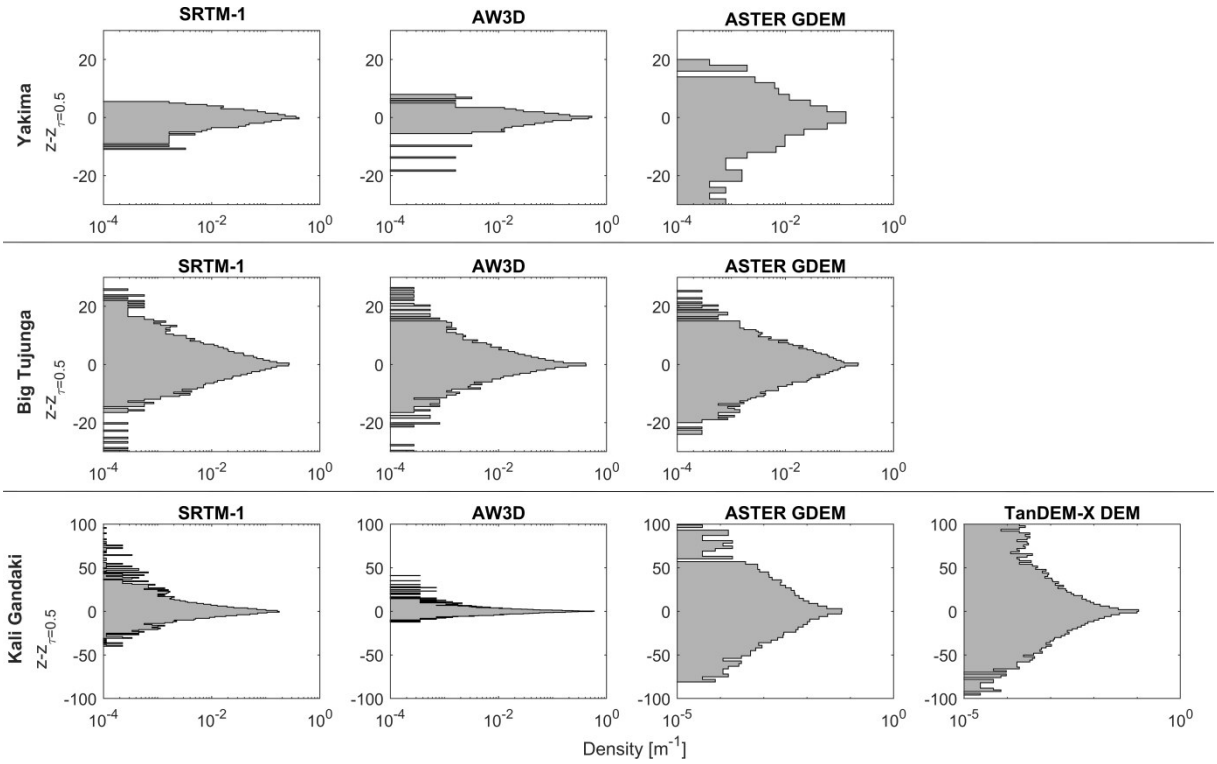

Fig. 3: Distributions of residuals derived from the CRS algorithm applied to different DEMs in the three study sites.

Page 9, Section 6.2: I think including analysis of channel slope and curvature may be needed in order to compare the ability of the different DEM datasets to analyse topographic information. Although elevation may not vary much with grid resolution, parameters such as local slope and curvature have been shown to be very sensitive to grid resolution (e.g. Vaze et al., 2010 (Env. Modelling and Software); Grieve et al., 2016 (ESurf)), with the range of slope and curvature values decreasing with resolution.

This is an issue that Reviewer 1 also addressed. Indeed, particular applications in tectonic geomorphology are often rather interested in along-river gradients than in elevations. To address this issue, our revised manuscript contains an additional section on how the CRS algorithm will affect river gradients. An analysis of data from the Yakima catchment shows that CRS is able to considerably narrow down the pixel-by-pixel differences between along-river gradients derived from a resampled LiDAR DEM and those obtained from CRS as compared to other methods.

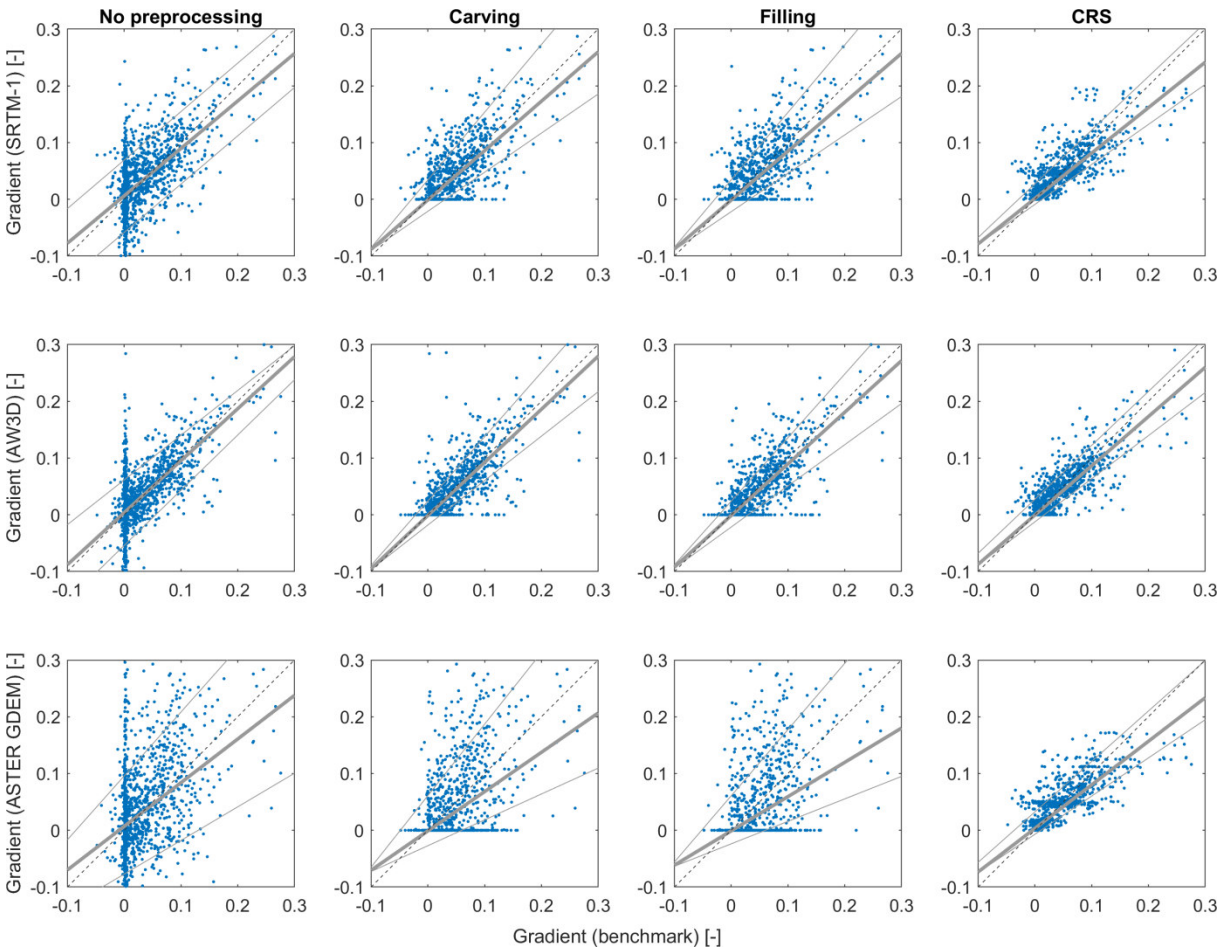

Fig. 4: Comparison of pixel-by-pixel along-river gradients derived from benchmark LiDAR DEMs (resampled to 30 m) and global DEMs in the Yakima catchment. Negative gradients in the benchmark and unprocessed DEMs are due to erroneously increasing river elevations in downstream direction. The grey solid lines (thin lines: 10 and 90%iles, thick line: median) are derived from a quantile regression. The dashed line is a one-to-one reference line. The parameters of the CRS algorithm (tau and K) are those in Table 4 of the manuscript. Compared to the original profiles and those obtained by preprocessing techniques filling and carving, the CRS algorithm is able to reduce the differences between along-river gradients as indicated by the narrow interquantile (90-10%iles) range.

Analysis of elevation values alone may suggest that the TanDEM-X dataset is not an improvement on the 30m datasets, but the higher resolution dataset may actually be more useful for extraction of these other metrics which are also important for channel profile analysis.

We rewrote this sentence to emphasize the potentials of TanDEM-X DEMs.

> ***The resolution of 12 m and high accuracy on hillslopes of the TanDEM-X DEM (Purinton and Bookhagen, 2017) will offer new opportunities, but whether and how TanDEM-X DEMs will offer any advantage for the analysis of river profiles in high mountain areas compared to previous DEMs with lower resolution needs further study.***

Page 10, Section 6.3: In general I like the title, and I get the idea of the good, bad, and ugly errors, but I think it could be expanded on a bit more - the authors should clarify here why random errors are good, and systematic errors are bad (can state more clearly that random errors are easier to smooth from the profile, whereas systematic errors are more difficult to distinguish from real signals).

We have rewritten this section and avoided the terms good, bad, and ugly. Please also see the reply to a comment from Reviewer 1.

Page 10, Section 6.4: I think some of this section makes more sense to have in the introduction to set the context of why developing the CRS algorithm is important.

We added the following sentence at the end of the introduction:

> ***Our algorithms will aid the visual interpretation and automated analysis of longitudinal river profiles and has additional applications in hydrodynamic modelling.***

Technical corrections

Page 2, Lines 19-20: I'd suggest rewording this sentence - it's unclear at the moment. Do you mean that random errors may or may not be clustered spatially?

We have reworded this sentence:

> ***"Random errors may also be autocorrelated, i.e., they cluster spatially (Oksanen and Sarjakoski, 2006)."***

Page 6, Line 15: rephrase sentence 'Thus derived profiles are monotonously decreasing downstream while filtering the wiggles'

We don't really see how to rephrase the sentence.

Page 9, Line 16-18: Split this into two sentences.

Done as requested:

> ***"However, this may depend on location as the ASTER GDEM quality is sensitive to a number of issues that may vary spatially. This includes the number of stacked stereo-pair scenes for the DEM generation, as well as land and cloud cover, water masking and registration quality (Purinton and Bookhagen, 2017)."***

Appendix A3: Equation wrongly labelled, should be A12.

Yes, this has been corrected now.

References:

De Smith, M.J., Goodchild, M.F., Longley, P. (2007): Geospatial analysis: a comprehensive guide to principles, techniques and software tools. Troubador.

Bumps in river profiles: uncertainty assessment and smoothing using quantile regression techniques

Deleted: the good, the bad,

Deleted: the ugly

Wolfgang Schwanghart[1], Dirk Scherler[2,3]

[1] University of Potsdam, Institute of Earth and Environmental Science, 14476 Potsdam-Golm, Germany
[2] GFZ German Research Centre for Geosciences, Earth Surface Geochemistry, 14473 Potsdam, Germany
[3] Freie Universität Berlin, Institute for Geological Sciences, 12249, Berlin, Germany

Correspondence to: Wolfgang Schwanghart (w.schwanghart@geo.uni-potsdam.de)

Abstract. The analysis of longitudinal river profiles is an important tool for studying landscape evolution. However, characterizing river profiles based on digital elevation models (DEM) suffers from errors and artifacts that particularly prevail along valley bottoms. The aim of this study is to characterize uncertainties that arise from the analysis of river profiles derived from different, near-globally available DEMs. We devised new algorithms – quantile carving and the CRS algorithm – that rely on quantile regression to enable hydrological correction and uncertainty quantification of river profiles. We find that globally available DEMs commonly overestimate river elevations in steep topography. The distributions of elevation errors become increasingly wider and right-skewed if adjacent hillslope gradients are steep. Our analysis indicates that the AW3D DEM has the highest precision and lowest bias for the analysis of river profiles in mountainous topography. The new 12-m resolution TanDEM-X DEM has a very low precision, most likely due to the combined effect of steep valley-walls and the presence of water surfaces in valley bottoms. Compared to the conventional approaches of carving and filling, we find that our new approach is able to reduce the elevation bias and errors in longitudinal river profiles.

1 Introduction

Rivers play a dominant role in the topographic evolution of the Earth surface, and possibly other planetary bodies (Hack, 1957; Howard, 1998; Whipple et al., 2013). They transfer sediment from mountains to depositional basins, set the base level for hillslopes, and convey tectonic and climatic signals across landscapes. The geometry of a river and specifically its longitudinal profile, reflect the climatic and tectonic forcing, variations in base level and sediment transport processes as well as differences in bedrock erodibility. Gradients along rivers, for example, reflect spatial variations in uplift rates (Whipple et al., 2013; Mudd et al., 2014; Scherler et al., 2014) and indicate the extent of past glaciations (Brardinoni and Hassan, 2006). Moreover, they can act as predictors for the zones of erosion and sediment accumulation during extreme events (Devrani et al., 2015) and reflect the repeated impact of masswasting events (Korup, 2006). Longitudinal river profiles and metrics derived them (e.g., the normalized channel steepness metric k_{sn} (Wobus et al., 2006)) have become

important tools for studying the topographic evolution of mountain belts and deciphering changes in climate and tectonics (Bishop et al., 2005).

Data on longitudinal river profiles are usually derived from digital elevation models (DEM) (Gonga-Saholiariliva et al., 2011; Wobus et al., 2006). Different sensors and techniques such as radar imaging, stereoscopy of optical imagery, terrestrial and airborne laser scanning, and structure-from-motion (SfM) provide DEMs at ever-increasing spatial resolution with unprecedented coverage. However, DEMs contain errors due to uncertainties in data acquisition, interpolation techniques and spatial resolution (Fisher and Tate, 2006; Purinton and Bookhagen, 2017). Structures such as bridges, culverts and reservoirs affect longitudinal river profiles derived from DEMs in ways that can either hide features present in reality or introduce patterns that do not represent the actual course of the profile (Schwanghart et al., 2013). Deviations from graded river profiles may reflect signals of climatic or tectonic perturbations, but often they relate to errors and artifacts that generate bumpy river profiles and thus introduce uncertainties that may compromise the interpretation of longitudinal river profiles (Harbor et al., 2005; Hayakawa and Oguchi, 2006; Wobus et al., 2006).

The objective of this study is to characterize and quantify the uncertainties of elevation values in longitudinal river profiles derived from near-globally and publicly available DEMs including the new TanDEM-X DEM (Wessel, 2016). To attain this goal, we devise new algorithms (quantile carving and constrained regularized smoothing) that use non-parametric quantile regression for assessing uncertainties and smoothing of river profiles. Using LiDAR DEMs as benchmark data and our new algorithms, we study how longitudinal river profiles derived from globally available DEMs (Table 1) are affected by errors and how these errors depend on the topographic setting. Moreover, we examine the best choice of parameter values for our algorithms to guide their application. Our algorithms will aid the visual interpretation and automated analysis of longitudinal river profiles and has additional applications in hydrodynamic modelling.

Deleted: as well as differences in bedrock erodibility. The analysis of longitudinal river profiles has therefore become an important tool

Deleted: existing

Deleted: Ultimately, these

Deleted: . We devised a new algorithm that uses

Deleted: algorithm

2 DEM artifacts and the longitudinal river profile

DEMs are the product of a processing chain that converts spatially discrete altitude measurements into a simplified representation of the Earth surface (Wechsler and Kroll, 2006). The processing chain typically involves ground-based, airborne, or satellite-based data acquisition, post-processing, and georeferencing. Subsequent interpolation and filtering operations usually convert these measurements into gridded datasets (Fisher and Tate, 2006). Because each processing step contains assumptions and analytical uncertainties, DEMs are not perfect representations of the land surface but contain errors that propagate through DEM-derived products (Fisher and Tate, 2006; Holmes et al., 2000; Reuter et al., 2009; Schwanghart and Heckmann, 2012).

DEM errors are either random or systematic. Random errors typically occur due to uncertainties related to instrument precision. Radar-derived DEMs, for example, include speckle and thermal noise as well as timing and positioning errors (Falorni et al., 2005; Rizzoli et al., 2012). Random errors may also be autocorrelated, i.e., they cluster spatially (Oksanen and Sarjakoski, 2006). Systematic errors are specific to the type of acquisition method. Lens distortions may affect DEMs

Deleted: spatially random or

Deleted:), i.e., they cluster spatially.

generated from both photogrammetric and SfM methods (James and Robson, 2014). Foreshortening, layover, and shadowing produce errors and voids in radar-derived DEMs (Falorni et al., 2005). Systematic errors are also found in DEMs interpolated from topographic contour lines (Guth, 1999; Wobus et al., 2006). While random errors tend to hide deterministic structure in the data, systematic errors may lead to wrong interpretations inferred from structures not present in reality.

Providers of DEM data usually describe the accuracy of their product through comparison with ground control points. More detailed error analyses, however, reveal the spatial variability of height errors in DEMs (Gorokhovich and Voustianiouk, 2006; Scherler et al., 2008). Global accuracy statistics are thus often insufficient to inform about the uncertainties of DEMs (Carlisle, 2005) and may lead to grave underestimation of the uncertainties in DEM-based modelling results (Canters et al., 2002; Hancock et al., 2006; Nardi et al., 2008).

Rivers present only a minor portion of the cells in a DEM, but this portion is particularly prone to certain types of errors (Guth, 2006; McMaster, 2002). Elevation anomalies along valley bottoms of the Pieniny Mountains, Poland, were found to range from -39 m to +145 m in the X-band SRTM and in the ASTER GDEM from -52 m to +88 m (Czubski et al., 2013; Ludwig and Schneider, 2006), thus vastly exceeding reported DEM accuracies (Jarvis et al., 2008; Tachikawa et al., 2011). Low DEM accuracy along rivers and valley bottoms can have several causes. In steep terrain, shallow viewing angles of radar systems can lead to shadow-related data loss. Although this problem can be mitigated by combining data from ascending and descending paths, it often cannot be completely eliminated (e.g., Rabus et al., 2003), and leads to systematically higher valley bottom altitudes in the C-Band SRTM DEM compared to the ASTER GDEM (Hayakawa et al., 2008). Difficulties in penetrating through thick riparian vegetation cause additional problems with DEMs derived from radar systems (Baade and Schmullius, 2014) and optical imagery (Gesch et al., 2012). As a consequence, patches of dense floodplain vegetation are likely to increase DEM values along river reaches, in particular where they are narrow. Although LiDAR derived DEMs often comprise benchmark data in terms of accuracy and resolution, gridded elevations along valley bottoms may still contain errors due to specular reflection and signal absorption by water (Malinowski et al., 2016).

In addition, DEM resolution limits the accurate representation of valley bottom heights. Where valley bottom width is less than twice the pixel size, DEMs may not capture the actual cross sectional shape correctly (Hengl, 2006). Finally, DEMs are simply unable to represent embankment underpasses such as bridges or culverts (Lindsay and Dhun, 2015). Unless manually or automatically removed, these features appear as positive excursions in the longitudinal river profiles, particularly at high spatial resolution (LiDAR-derived DEMs) and in human-altered landscapes (Schwanghart et al., 2013; Sofia et al., 2013).

Accurate representation of drainage structures can be obtained by algorithms that interpolate DEMs from scattered data points and contour lines (Hutchinson et al., 2011). Most of the above-mentioned errors, however, cannot be avoided during DEM generation and require post-processing steps. Flow path enforcement (Lindsay, 2016) is a class of algorithms to establish flow connectivity between all pixels within a DEM and its edges. While these algorithms primarily adjust planform flow patterns, they can also be used to modify DEM values. For example, *flood filling* of sinks ensures that each pixel has at least one neighboring pixel with equal or lower elevation (Fig. 1a). The drawback of this approach is that it creates

Deleted: 1

potentially large flat areas where topographic information is lost, and that it leads to unrealistic flow patterns imposed on the filled topography (Soille et al., 2003) that ultimately affect longitudinal river profiles (Watson et al., 2015). In contrast, *carving* (Fig. 1b), is a procedure to cut through blockages, typically by imposing the constraint that while moving downstream, no pixel is higher than its upstream neighbors (Lindsay, 2016; Schwanghart et al., 2013; Soille et al., 2003). In addition, there exist combinations of carving and filling that minimize the costs (i.e., measured by the total amount of DEM modifications) of transforming the DEM during flow enforcement (Lindsay, 2016; Soille, 2004). However, no matter which flow enforcement approach is used, the derived river profiles will most certainly contain zero-gradient sections (Nardi et al., 2008) with abrupt steps at their downstream facing side. Distinguishing such "artificial riffle-pool sequences" from actual ones is often not easy (Hayakawa and Oguchi, 2006).

Common approaches for removing errors in river profiles include running average filters (Hayakawa and Oguchi, 2006), contour-interval subsampling (Wobus et al., 2006), smoothing splines (Harbor et al., 2005), and locally weighted regression (Aiken and Brierley, 2013). However, all of these approaches face similar problems: they fail to remove spikes if the length of the moving window is too small and average out potentially important features if the window is too large (Aiken and Brierley, 2013). Furthermore, conventional smoothing algorithms are typically applied to individual river reaches rather than entire river networks, which may lead to sharp discontinuities at river confluences. Finally, even robust approaches that aim at reducing the influence of individual outliers on the smoothed curve (Aiken and Brierley, 2013) may yield profiles that contain sections with downstream increasing elevation that result from long sections where valley bottom elevations are overestimated. An example of how outliers may generate downstream increasing elevations in profiles smoothed by a running average is shown in Fig. 1c. Harbor et al. (2005) used an iterative procedure that lowers downstream locations and raises upstream locations to correct such sections but thus produced river profiles may not be consistent with the data.

What is thus needed is an approach that (i) filters DEM artifacts from longitudinal river profiles while ensuring downstream decreasing elevations, and that (ii) accounts for the fact that river elevations are usually overestimated. Moreover, the approach should be applicable to entire river networks instead of single rivers only, and should be flexible enough to deal with breaks in along-river slopes where these actually exist.

3 The CRS algorithm

We wish to transform a bumpy river profile into a smoother profile so that it ideally contains elevations and along-river gradients that approximate those in reality. Common approaches such as the running average and local regression – possibly combined with flow enforcement techniques – insufficiently cope with systematic biases and outliers, and may even produce profiles that increase in downstream direction (Fig. 1). Our approach avoids these drawbacks and combines flow enforcement and smoothing in one procedure.

We developed a non-parametric quantile regression that we term CRS (constrained regularized smoothing) algorithm. Our approach exploits the network topology of river networks (see Appendix A1) and estimates the τth quantile function $Q_{z|x}(\tau)$

Deleted: 1

Deleted:

Deleted: ,

Deleted: ,

Deleted: .

Deleted: elevations

Deleted: (

Deleted: 1).

of the random variate elevation Z conditional on the distance X in the upstream direction from the outlet. We chose a quantile regression rather than a least squares approach (see Appendix A2) despite the computational appeal of least squares. Quantile regression makes no assumptions about the underlying probability distribution of the observational noise and is more robust to outliers. Moreover, quantile regression provides the opportunity to obtain a comprehensive estimate of the distribution of Z (Koenker, 2010) and is therefore suited to applications that are interested in more than the mean as a single sample.

We propose a non-parametric approach to regression so that the river profile does not take a predetermined shape. River profiles are usually too variable to be characterized by a functional model (e.g. the stream power model) and any strict assumptions about profile form, e.g. a concave upward steady state profile, would limit the range of potential profiles the algorithm could be applied to (Shepherd, 1985). In turn, a non-parametric free-form solution entails the inference of a very large number of parameters. In fact, there are as many parameters as elevation values in the profile, such that the problem is ill-posed. Regularization refers to the approach to include additional constraints to the solution of the problem. Here we use regularization to encode preference for local smoothness and spatial autocorrelation (Sivia and Skilling, 2006) of the river profile, an assumption that is vital for any kind of spatial analysis (De Smith et al., 2007). Given that there is usually only one realization of Z for each value of X, assumptions about local smoothness are indeed necessary to make any statements about the distribution of $Z(X)$. However, this requirement can be relaxed if we force profiles to decrease in downstream direction. Here we first show how such a monotonicity constraint leads to an approach that we term *quantile carving* before we proceed with the CRS algorithm.

Deleted: .

Commonly, quantiles are derived by sorting data and determining the values that separate the data into the desired proportions. However, quantiles can also be defined as an optimization problem of minimizing a sum of symmetrically (in case of the median) or asymmetrically weighted absolute residuals (Koenker, 2010). If the τth quantile function is $Q_z(\tau) = Iz_\tau$ with I being the identity matrix, then z_τ is found by minimizing the argument

$$\arg\min \sum_{i=1}^{n} \left(\rho_\tau(z - Iz_\tau)\right) \quad (1)$$

where ρ_τ is the loss function

$$\rho_\tau(z - Iz_\tau) = (z - Iz_\tau)(\tau - \mathbb{I}_{(z-Iz_\tau)<0}) \quad (2)$$

and $\mathbb{I}$ is an indicator function that has a value 1 if $(z - Iz_\tau) < 0$ and 0 otherwise (Koenker, 2010). At this point, however, z_τ is not conditional on distance x, but calculated independently for each point along the river profile. Unless multiple samples exist for each location, which is usually not the case, z_τ equals z. However, we can explicitly condition z_τ by adding prior knowledge about river geometry, i.e., by constraining elevations to be monotonously decreasing downstream ($z_\tau(x)$ is greater or equal than any downstream elevation). Formally, this is achieved by minimizing eq. (1) subject to the inequality constraint $z_\tau(x) \geq z_\tau(x - \delta x)$ which is a minimization problem that can be solved by linear programming methods

(Koenker, 2010) (see Appendix A3). We refer to this approach of processing the longitudinal river profile as *quantile carving* and show examples of its application in Fig. 2. For quantiles approaching 0 and 100%, the resulting profiles will follow those of the commonly used hydrological conditioning approaches carving and filling, respectively. Thus, carving and filling are extremal approaches and quantile carving provides a statistical framework that links the two.

A disadvantage of the commonly applied techniques of carving and filling is that they often introduce zero-gradient sections in the profile that are typically separated by artificial steps (Fig. 1). The same applies to quantile carving and disrupts our aim of a realistic representation of the river profile (Fig. 2). A smoother profile is characterized by less local variability and is devoid of sharp kinks. Given a longitudinal river profile, there are many ways of measuring how rough or wiggly the profile is. An intuitively appealing measure is the integrated second derivative $\int [z_\tau{}''(x)]^2 dx$ which is not affected by the addition of a constant or linear function and has considerable computational advantages (Green et al., 1993). The CRS algorithm expands on quantile carving by determining the cost of a particular solution not only by its goodness-of-fit, but also by its roughness. This entails additionally minimizing the integrated second derivative so that the optimization involves a quadratic problem:

$$\arg\min \sum_{i=1}^{n} \left(\rho_\tau(z(x) - Iz_\tau(x))\right) + s \int [z_\tau{}''(x)]^2 dx \quad \text{subject to } z_\tau(x) \geq z_\tau(x - \delta x) \tag{3}$$

The scalar s determines the weight of the integrated second derivative and is calculated by Eq. (4) where Δx is the spatial resolution of the DEM, n is the number of nodes in the network and p is the number of second derivative equations:

$$s = (\Delta x)^2 K \sqrt{\frac{n}{p}} \tag{4}$$

Larger values of the smoothing parameter K result in smoother profiles (Fig. 3). We include the squared spatial resolution into the equation so that any linear transformation (e.g. distance scaling) of the river profile does not affect the smoothing results. Yet, this entails that profiles with different spatial resolutions must be smoothed with different values of K to obtain the same or at least similar results. If two profiles A and B have different spatial resolutions Δx_A and Δx_B, then smoothing both profiles will return similar results if the smoothing parameter K_B is calculated from K_A by Eq. (5).

$$K_B = \left(\frac{\Delta x_A}{\Delta x_B}\right)^2 K_A \tag{5}$$

The quadratic term in Eq. (3) renders the optimization problem suitable for quadratic programming (Takeuchi et al., 2005). By formulating the CRS algorithm as a quadratic programming problem (see Appendix A4), we obtain high flexibility for setting and relaxing constraints on the resultant profiles. For example, we may want to force elevations at particular locations

to take on predefined values that were measured in the field and are precisely known. In other locations such as waterfalls and rapids, dams, or river confluences, profiles may actually exhibit high curvatures that should remain in the smoothed profile. Provided that these locations are precisely known, the curvature constraint can be locally relaxed or entirely removed by setting variable values of K. Thus, unlike previous approaches, the CRS algorithm allows for incorporating prior knowledge about river-profile geometry and independent observations.

Longitudinal river profiles of the Big Tujunga catchment (San Gabriel Mountains, USA) and derived from the SRTM-1 are shown in Fig. 3. The profile values show large fluctuations that are particularly high in the central part of the profile where hillslope gradients adjacent to the river are highest. Results of the CRS algorithm for different values of K and τ are shown in Fig. 3b-e. Thus derived profiles are monotonously decreasing downstream while filtering the wiggles. The amount of smoothing is dictated by K. For K=1 and τ = 0.5, the profile contains various steps and these steps remain for different values of τ. A higher value of K more effectively filters the profile, but strongly influences the range between the 10^{th} and 90^{th} percentiles at some locations. The tributary in Fig. 3d and e lacks the small scale variability such that the interquantile range derived with K=1 is very low compared to K=10. Any uncertainty estimate based on the interquartile range must thus depend on K.

4 Methods and data

Our goal in this study was to (1) assess the quality of near-globally and publicly available DEMs (hereafter termed global DEMs) for the analysis of longitudinal river profiles, and to (2) examine the best choice of parameter values of the CRS algorithm and compare its performance with commonly used approaches filling and carving. This allows us to report ranges of parameter values that will guide the application of the CRS algorithm in other areas.

We addressed the first point by comparing river profiles obtained from global DEMs (SRTM-1, ALOS World 3D30 (AW3D), ASTER GDEM v2, TanDEM-X DEM) (see Table 1, Fig. 4). Our test sites are the Yakima catchment in the undulating to hilly landscape of the Washington Mountains, USA, the Big Tujunga catchment in the hilly to mountainous landscape of the San Gabriel Mountains, USA, and the Kali Gandaki catchment in the mountainous landscape of the High and Lesser Himalayas, Nepal. The TanDEM-X DEM is available to us only for the Kali Gandaki catchment. We first compared the global DEM with those of LiDAR DEMs, where available, to obtain estimates of absolute errors. The LiDAR DEMs are bare-earth DEMs derived from point clouds (>3 points/m^2) and were downloaded from the OpenTopography facility (Table 1). Due to their decimeter to sub-decimeter accuracy, we consider the LiDAR data as our benchmark DEMs. The acquisition dates of the DEMs vary but we expect that temporal changes in the land surface are minor. We used the reference ellipsoid defined by the world geodetic system WGS 84 as basis for all DEMs and resampled them to the same spatial extent and resolution (30 m) using bilinear interpolation. We then derived flow directions and stream networks for selected channel heads from the downsampled LiDAR DEMs, and obtained elevations along those networks from the global DEMs. This approach may overestimate errors in DEMs due to resampling and because lateral patterns of stream networks

Deleted: We calculated ellipsoidal heights (WGS84)

derived from different DEMs may differ. However, 2D crosscorrelation of global DEMs with the LiDAR DEMs did not reveal any systematic horizontal shifts between the DEMs. Due to the lack of benchmark data, we could not quantify absolute errors for the Kali Gandaki. Thus, we next determined relative errors (precision) along the river profiles by smoothing the profiles with the CRS algorithm. We chose the median ($\tau = 0.5$) to obtain profiles along the local central tendency of the data and set the smoothing parameter $K=5$ which we found by visual analysis suitable to filter the data while sufficiently reproducing the structure of the profiles. We quantified the precision using the deviations of the profiles from the CRS-smoothed profiles. Because the study site in Nepal represents a cross-section through the Himalaya with pronounced differences in topographic relief, we also assessed the spatial variability of precision as moving down the river. Specifically, we tested whether median hillslope gradients within a distance of 1000 m of the Kali Gandaki exert any influence on the precision of river profiles.

To address the second point of our study, we used a derivative-free simplex search method to find values of the parameters K and τ that yield CRS-smoothed profiles that best approximate the LiDAR-derived profiles. Since a good agreement of profiles is largely determined by both similar elevations and gradients, we defined the objective function f to be minimized as a function of the elevation ($z_{i\Delta}$) and gradient offsets ($g_{i\Delta}$) between the profiles

$$f(z_{i\Delta}, g_{i\Delta}) = \sum_i (z_{i\Delta} g_{i\Delta})^2 \qquad (6)$$

Again, we have to restrict our analysis to the Yakima and Big Tujunga catchments due to the unavailability of benchmark data for the Kali Gandaki catchment.

Finally, we analyzed the sensitivity of profiles derived by the CRS algorithm to changes of the values K and τ. Specifically, we studied how variations of both parameters affect the goodness of fit between pixel-by-pixel elevations as well as along-river gradients derived from the smoothed profiles and the LiDAR benchmark DEMs.

We implemented the proposed algorithms in TopoToolbox 2 (see also Appendix B), which is software for the analysis of DEMs (Schwanghart and Scherler, 2014). The software is written in MATLAB and thus has direct access to a numerical library of optimization routines usually lacking in standard GIS software. To minimize equations (1) and (3), we used the function linprog and quadprog of the MATLAB optimization toolbox which solve linear and quadratic problems, respectively (see also Appendix A1-4).

5 Results

Elevation offsets between the global DEMs and the LiDAR data differ in-between sites and DEM types (Fig. 5). All river profiles are consistently biased towards higher altitudes compared to the LiDAR data (Table 2), but more so in the steeper terrain of the Big Tujunga catchment compared to the Yakima dataset. The observed bias does not affect the entire DEM but approaches zero on hillslopes (Fig. 6) so that we infer that low accuracy particularly affects valley bottoms. Based on kernel-derived probability density distributions, the quantiles of the zero offset are less than the median (except for AW3D in

Yakima), and again lower in steep terrain. Despite predominant overestimation, negative offsets also exist and have minimum values that range from -3 to -45 m. We observe maximum absolute deviations of up to 49 m that are usually positive as indicated by positive skewness values for the SRTM-1 and AW3D datasets. An exception is the ASTER GDEM where offsets are inconsistently skewed towards positive and negative values. In general, the differences between the ASTER GDEM-derived and LiDAR-derived profiles are highly variable as indicated by a high standard deviation in both sites.

Deviations between the original and CRS-smoothed profiles from global DEMs further highlight errors in profiles obtained from different DEMs at different sites, including the site in Central Nepal where LiDAR data is unavailable (Fig. 7). With increasing topographic relief, residuals from the median profile are increasingly biased towards positive values (Table 3). At the same time, the higher root mean squared error (RMSE) shows that increasing relief results in a reduced precision. Elevation values from the AW3D dataset show the highest precision at all sites whereas the TanDEM-X DEM has the highest RMSE (Table 3, Fig. 8). Note that we only took those elevation values from the TanDEM-X DEM into account that are flagged to be consistent, as indicated in the consistency mask that is provided together with the DEM data (Wessel, 2016).

The above observations beg the question of what topographic parameters control the precision of longitudinal river profiles. Our data from Central Nepal show that error magnitudes, estimated as the 95-5% interquantile range, vary spatially (Fig. 9). In particular, there exist sections along the Kali Gandaki River where elevations derived from all DEMs have low precision (Fig. 9a, b). Hillslope gradients within 1000 m distance from the river, measured and averaged within 10-km-long river reaches, correlate with precision (Fig. 9c). This indicates that all DEMs have problems to precisely represent the bottom of valleys straddled by steep canyon walls. Again, the precision differs strongly between the DEMs with ASTER GDEM and TanDEM-X DEM having the lowest precision.

Based on the LiDAR data from the Yakima and Big Tujunga catchments, we found different optimal values of K and τ for the different DEMs (Table 4). Values of K and τ are particularly large for the ASTER GDEM, which is quite noisy along the Yakima River. τ values are always less than 0.5 and lower in the Big Tujunga which is consistent with the percentile value τ_0 (0.01-0.55) determined before (Table 2). In general, the CRS algorithm reduces the deviations from the benchmark profile by lowering the RMSE by a factor of 1.4-2.0. Compared to profiles derived from the carving and filling algorithms, CRS algorithm yields considerable lower RMSE.

The improved agreement between the profiles derived from the CRS algorithm is also reflected by a higher pixel-by-pixel correlation of gradient of CRS derived profiles and those of the benchmark DEMs. Fig. 10 shows a comparison of gradients derived from the global DEMs and by preprocessed by different methods for the Yakima catchment. Profiles without preprocessing exhibit the largest scatter. The scatter is most effectively decreased by the CRS algorithm as it reduces the number of zero gradients and artificial steps as compared to the methods filling and carving.

Figure 11 illustrates the results from a sensitivity analysis of the CRS-derived profiles to changes in K and τ for the Yakima catchment and the AW3D DEM. The sensitivity analysis shows that increasing values of K can excessively smooth the

Deleted: .

Deleted: 8

Deleted: 8a

Deleted: 8c

Deleted:

profile and thus impair the agreement between the profile elevations and gradients. Very low (<0.01) and high (>.099) values of τ can also lead to grave mismatches of the smoothed profile and the benchmark profile as the quantile approach fails to penalize large deviations as opposed to a least-squares approach. The analysis also shows that an agreement between elevations or slopes is not necessarily derived from the same set of parameter values. Whereas an agreement of elevations is largely obtained by varying τ in a rather broad range of K between 0.1 to 3 (Fig. 11a), an agreement of gradients is largely within a narrow range of K and a broad range of τ between 0.3 and 0.8 (Fig. 11b). Fitting profiles to benchmark data may thus significantly depend on whether the objective function minimizes the differences between river elevations or gradients (Fig. 11c).

6 Discussion

6.1 Positive bias of elevation in river profiles

Different methods of data acquisition and DEM generation have in common that DEM errors along valley bottoms are usually biased towards positive values (Hayakawa and Oguchi, 2006). Our analysis shows that this bias is more pronounced in steep terrain, which calls for caution when interpreting longitudinal river profiles in mountainous landscapes. The bias may at least partly be due to the coarse resolution that averages over finer-scale topographic variability. As we resampled our benchmark LiDAR DEM to the resolution of our tested DEMs and still large differences to global DEMs exist, additional causes of the observed bias must exist that relate to the type of data acquisition and field site characteristics (Vaze et al., 2010). While we cannot resolve the underlying causes in detail, our results suggest that biases affect all DEMs, although to different degrees.

Deleted: , however

Deleted: .

6.2 Precision of river profiles derived from global DEMs

In addition to the bias, the distribution of elevation errors in the longitudinal river profiles becomes increasingly wider and right-skewed in landscapes of higher relief. As relief increases, the profiles obtained from all global DEMs have decreasing precision, but there is a more than five-fold difference between the precision of the different DEMs. In all three sites, the AW3D dataset has the highest precision, followed by the SRTM-1: a finding that is consistent with other DEM assessments (Purinton and Bookhagen, 2017). The precision of the ASTER GDEM is particularly low compared to SRTM-1 (Czubski et al., 2013) and AW3D. However, this may depend on location as the ASTER GDEM quality is sensitive to a number of issues that vary spatially. This includes the number of stacked stereo-pair scenes for the DEM generation, as well as land and cloud cover, water masking and registration quality (Purinton and Bookhagen, 2017). In our study site in Nepal, the precision of river profiles derived from the TanDEM-X DEM is much lower than the reported 10 m absolute and 2 m relative height accuracy (Gruber et al., 2012a; Purinton and Bookhagen, 2017). Low accuracy along river profiles may relate to water bodies that are generally incoherent areas in the underlying DEM scenes and have height estimates that are known to be noisy and inaccurate (Wessel, 2016). The resolution of 12 m and high accuracy on hillslopes of the TanDEM-X DEM

Deleted: that were available

Deleted: and also

Deleted: However,

Deleted: the derived

Deleted: Despite its high spatial

Deleted: , our results suggest that

(Purinton and Bookhagen, 2017) will offer new opportunities, but whether and how TanDEM-X DEMs will offer any advantage for the analysis of river profiles in high mountain areas compared to previous DEMs with lower resolution needs further study (Gruber et al., 2012b).

Deleted: offers hardly

Deleted: . As we restricted our analysis of the TanDEM-X DEM to an area with extreme topography further studies are required to test whether our results are transferable to other sites (Gruber et al.,

6.3 Error distribution and the CRS algorithm

The asymmetric distribution of residuals around the median (and mean) violate the assumptions of methods for filtering height errors that rely on least squares such as local regression techniques. Moreover, the large absolute values of outliers further complicate the application of methods that rely on averaging (e.g. running average filters). Although positive bias is on average more common, our results show that 10-50% of the profile values underestimate the actual river elevation. This underscores potential problems with using carving to hydrologically trim DEMs. Our new quantile-carving and CRS algorithms implement a quantile regression that remains largely unaffected by skewed data and outliers, and thus prevents that very low or high values gain excessive weight for shaping the longitudinal profile.

Our comparison of river profiles derived from global DEMs with those derived from LiDAR shows that CRS-smoothing of river profiles can decrease differences to actual river elevations and gradients compared to commonly used methods of filling and carving. We derived an optimal value of the smoothing parameter K by comparing the smoothed profiles with LiDAR data that were available for subsets of the data and this may be a common approach where high-resolution, precise and accurate data is available for parts of the study area. Where such data is unavailable the most suitable value of K depends on the amount of scatter in the profiles, the true roughness (e.g., riffle-pool sequences in bedrock rivers vs. relatively smooth profiles of alluvial rivers), but also the type of application. One-dimensional hydraulic simulations, for example, may retain some of the variability of channel gradients while attempting to avoid the influence of erroneous data, and thus choose a low value of K. In many applications, visual interpretation of profiles will aid the identification of suitable values of K and τ. More general, it may be pragmatic to let K be as large as possible while satisfying the constraints of the data (Sivia and Skilling, 2006). Although there exist ways to determine an optimal value of K by cross-validation approaches (Garcia, 2010), qualitatively and visually cross-checking may be the most practical approach in many cases: too small values of K will admit unnecessary and potentially erroneous structure whereas too large values impede a good agreement with the actual river profile (Sivia and Skilling, 2006).

6.4 Autocorrelated errors

River profiles are derived from measurements that give rise to errors of different types: random and systematic components, as well as artifacts (Reuter et al., 2009). We have shown that the CRS algorithm can efficiently handle random errors and may reduce offsets that arise from systematic or artefactual deviations between actual river profiles and those derived from DEMs, thus improving an overall representation of longitudinal river elevations and gradients. Caution, however, must be taken with autocorrelated errors that we have not addressed here although they may significantly affect river profiles. Autocorrelation entails that if the true elevation at some location is overestimated in the DEM, then the elevation at a nearby

Deleted: 6.3 The good, the bad, and the ugly?¶

Deleted: (the good ones)

Deleted: (the bad ones)

Deleted: .

Deleted: the ugly

Deleted: : the autocorrelated errors. If

pixel will likely also be overestimated (Temme et al., 2009). Autocorrelated errors have important consequences for the choice of smoothing parameters. In the case of short-range dependence, profiles may not be affected severely if a sufficiently large smoothness parameter is chosen. Long-range dependence, however, is neither easy to detect nor their structures simply removed by non-parametric regression. For example, it is difficult to ascribe the stepped patterns in Fig 3b to actual riffle-pool sequences or to artefacts that should be smoothed (Fig. 3c). Although approaches to nonparametric regression exist that are able to cope with autocorrelated errors (Opsomer et al., 2001), their implementation and assessment were, however, beyond the scope of this study. The CRS algorithm cannot differentiate actual steps in the profiles from artificial bumps. It smooths profiles to remove scatter and thus accentuates the actual patterns in the data. The quantile regression technique enables to derive uncertainty bounds which can support data interpretation by quantifying DEM errors.

Deleted:

Deleted: 4

6.5 Applications and future developments

The CRS algorithm can be used in various fields of research. Primarily, in studies of river profiles one may wish to remove noise from profiles while preserving underlying patterns and quantifying uncertainty. In tectonic geomorphology, for example, knickzones in longitudinal river profiles are essential proxies for transient river adjustment (Bishop et al., 2005), but distinguishing actual knickzones from data artifacts is challenging (Neely et al., 2017). Interquantile ranges determined by the CRS algorithm provide an objective way to determine minimum elevation drops that a knickzone must have to be identified against the background noise. Hydrodynamic simulations in mountainous environments frequently use globally available DEMs such as the SRTM or ASTER GDEM (Jarihani et al., 2015; Watson et al., 2015), but erroneous river profiles can introduce numerical instabilities (Paiva et al., 2011) and roughness, thus severely limiting the reliability of flood assessment, hazard zonation, and risk management (Watson et al., 2015). In a recent study on flash flood warning and hazard assessment in the Nepal Himalaya, a preliminary version of the CRS algorithm provided an important preprocessing step to improve the accuracy of estimating flow depth, flow speed, and flood wave arrival times (Bricker et al., 2017).

Applying quantile carving and the CRS algorithm is computationally more expensive compared to carving and filling. Run times depend largely on the number of nodes (or pixels) in a river network (Fig. 12). Thus, we applied our analysis to river networks only and not to entire DEMs, although this is principally possible provided convergent flow networks (O'Callaghan and Mark, 1984) have been derived. Rapid preprocessing of DEMs with our algorithms should apply parallelization strategies to allocate individual drainage basins or reaches to different processors. Future studies may also want to make use of the high flexibility of the algorithms. For example, values of the quantile τ and the smoothing parameter K could be set for individual pixels or river reaches, thus varying the amount of smoothing spatially. This may be useful if the true variability in river gradients shall be retained where these are known to vary strongly, e.g., as a function of upslope area or hillslope relief (Fig. 9). Finally, the CRS algorithm is not restricted to elevation profiles, but can also be applied to other variables measured or calculated along river profiles such as steepness (Ksn) or curvatures both of which are usually prone to even larger uncertainties.

Deleted: 9

Deleted: 8

Deleted: .

7 Conclusions

Comparison of longitudinal river profiles derived from coarse-resolution globally available DEMs and LiDAR data shows that DEMs commonly overestimate elevations along rivers in steep topography. Moreover, error distributions become increasingly wider and positively skewed if adjacent hillslope gradients are steep. Our analysis suggests that the AW3D DEM has the highest precision and lowest bias for the analysis of river profiles in mountain topography. In contrast, the 12 m resolution TanDEM-X DEM has a very low precision, most likely due to the combined effect of steep valley-walls and the presence of water in valley bottoms. To characterize and remove such systematic and random errors in DEMs, we developed the CRS algorithm for correcting and smoothing longitudinal river profiles. The approach adopts a non-parametric quantile regression and handles entire river networks instead of single river reaches, and ensures downstream decreasing elevations. Compared to the conventional approaches of carving and filling, we find that our new approach is able to reduce the elevation bias and errors in longitudinal river profiles.

Acknowledgments

We thank the German Aerospace Center (DLR) for granting access to TanDEM-X data as part of the project DEM_GEOL1053, and the OpenTopography Facility for providing a great platform for sharing LiDAR data and global DEMs. LiDAR data is based on services provided to the Plate Boundary Observatory by NCALM (http://www.ncalm.org). PBO is operated by UNAVCO for EarthScope (http://www.earthscope.org) and supported by the National Science Foundation (No. EAR-0350028, EAR-0732947, and EAR-1043051).

Appendix A:

A1 River network representation, and along-river gradient and curvature

We represent the river network as a directed acyclic graph $G(V, E)$ (Heckmann et al., 2015). The set of graph nodes V_i are pixel centers connected by directed edges $E(i, j)$. We denote the downstream node of i as j and the upstream node as k. While in general our algorithm is also applicable to divergent channel networks, i.e., braided or anastomosing rivers, as derived from multiple flow direction algorithms, we restrict our formulation to channel networks derived from the single flow direction algorithm (D8) (O'Callaghan and Mark, 1984). This restriction entails that G is a directed tree network (Ahuja et al., 1993) and each node i has no more than one downstream neighbor j and a maximum of eight upstream neighbors $k = \{1,2, \dots\}$ unless the node is the outlet or a channel head of the river network. We calculate the gradient of the river with forward finite differences

$$\frac{dz_i}{dx} = \frac{z_i - z_j}{x_i - x_j} \quad \text{(A1)}$$

so that positive gradients denote decreasing elevations in the downstream direction. In matrix notation, this equation is

$$\frac{d\boldsymbol{z}}{dx} = \boldsymbol{G}\boldsymbol{z} \quad \text{(A2)}$$

where elements on the main diagonal of $\boldsymbol{G}$ are $g_{ii} = \left(x_i - x_j\right)^{-1}$ and off-diagonal elements are $g_{ij} = -\left(x_i - x_j\right)^{-1}$.

We approximate the second derivative, i.e., the profile curvature, by the 2nd order central difference.

$$\frac{d^2 z_i}{dx^2} = \frac{dz_k - dz_i}{0.5\,(x_k - x_j)dx} \quad \text{(A3)}$$

Since pixel centers may be cardinally and diagonally linked and are thus unequally spaced, we rearrange and write this equation in matrix notation for a reach with three nodes centered at i

$$\frac{d^2 z_i}{dx^2} = \begin{bmatrix} \frac{2}{(x_i - x_j)(x_k - x_j)} & \frac{-2}{(x_k - x_i)(x_i - x_j)} & \frac{2}{(x_k - x_i)(x_k - x_j)} \end{bmatrix} \begin{bmatrix} z_j \\ z_i \\ z_k \end{bmatrix} \quad \text{(A4)}$$

or for all neighboring node triplets:

$$\frac{d^2\boldsymbol{z}}{dx^2} = \boldsymbol{C}\boldsymbol{z} \quad \text{(A5)}$$

where each row r in C refers to an individual node triplet such that $C_{rj} = 2/((x_i - x_j)(x_k - x_j))$, $C_{ri} = -2/((x_k - x_i)(x_i - x_j))$, and $C_{rk} = 2/((x_k - x_i)(x_k - x_j))$.

A2 Linear constrained regularized smoothing

A linear least squares approach to longitudinal river profile smoothing can be derived as follows based on the variables defined in Appendix A1. The approach uses a penalized least squares estimator that minimizes the sum of the squared residuals and its roughness at the same time. Given the roughness penalty $K>0$, the penalized sum of squares PSS is

$$PSS(z) = \sum_{i=1}^{n} [z_i - \hat{z}_i]^2 + s \int_x [\hat{z}_i'']^2 dx \quad \text{(A6)}$$

The parameter s determines the degree of exchange between the residual error and local variability of $\hat{z}$ and is calculated as

$$s = (\Delta x)^2 K \sqrt{\frac{n}{p}} \tag{A7}$$

from the smoothness parameter K, the spatial resolution Δx, the number of data points n and the number of second derivative equations p. In matrix notation, Eq. (A6) is written as an overdetermined system of equations

$$\begin{bmatrix} \boldsymbol{I} \\ s\boldsymbol{C} \end{bmatrix} \hat{\boldsymbol{z}} = \begin{bmatrix} \boldsymbol{z} \\ \boldsymbol{0} \end{bmatrix} \tag{A8}$$

or

$$\boldsymbol{A}\hat{\boldsymbol{z}} = \boldsymbol{b} \tag{A9}$$

where $\boldsymbol{0}$ is a vector of zeros with equal number of rows as $\boldsymbol{C}$. We then derive the regularized elevations by the general linear model:

$$\hat{\boldsymbol{z}} = (\boldsymbol{A}^{\boldsymbol{T}}\boldsymbol{A})^{-1}\boldsymbol{A}^{\boldsymbol{T}}\boldsymbol{b} \tag{A10}$$

The resulting elevations will not necessarily decrease monotonically downstream. We thus reformulate the linear model in eq. (A10) as a quadratic programming problem that minimizes a linear least squares system under the constraint of monotonically decreasing elevations downstream:

$$\min_{\hat{\boldsymbol{z}}} \frac{1}{2}\hat{\boldsymbol{z}}^{\boldsymbol{T}}\boldsymbol{H}\hat{\boldsymbol{z}} + \boldsymbol{f}^{\boldsymbol{T}}\hat{\boldsymbol{z}} \text{ such that } \begin{cases} -\boldsymbol{G}\hat{\boldsymbol{z}} \leq -\boldsymbol{g}_{min} \\ \boldsymbol{I}_{\boldsymbol{eq}} \cdot \hat{\boldsymbol{z}} = \boldsymbol{z}_{\boldsymbol{eq}} \\ \boldsymbol{lb} \leq \hat{\boldsymbol{z}} \leq \boldsymbol{ub} \end{cases} \tag{A11}$$

where the superscript $\boldsymbol{T}$ refers to the transpose, $\boldsymbol{H} = 2\boldsymbol{A}^{\boldsymbol{T}}\boldsymbol{A}$ is a quadratic positive definite matrix and $\boldsymbol{f} = -2\boldsymbol{A}^{\boldsymbol{T}}\boldsymbol{b}$ represents the linear term. $\boldsymbol{I}_{\boldsymbol{eq}}$ is a n-by-n matrix with ones on the main diagonal for nodes whose smoothed elevations must equal the values in $\boldsymbol{z}_{\boldsymbol{eq}}$. All other elements in $\boldsymbol{I}_{\boldsymbol{eq}}$ and $\boldsymbol{z}_{\boldsymbol{eq}}$ are zero. The linear constraint that $-\boldsymbol{G}\hat{\boldsymbol{z}} \leq -\boldsymbol{g}_{min}$ ensures that elevation gradients at all nodes are equal or greater than $\boldsymbol{g}_{min}$. Setting $\boldsymbol{g}_{min} < 0$ will return longitudinal river profiles that are strictly monotonically downstream decreasing. The vectors $\boldsymbol{lb}$ and $\boldsymbol{ub}$ define lower and upper bounds of $\hat{\boldsymbol{z}}$, respectively.

A3 Quantile carving

Equation 1 can be efficiently solved by linear programming. Linear programming finds the vector $\boldsymbol{x}$ that minimizes $f^T\boldsymbol{x}$ subject to linear inequality ($\boldsymbol{Ax} \leq \boldsymbol{b}$) and equality constraints ($\boldsymbol{Aeq}\ \boldsymbol{x} = \boldsymbol{beq}$) and lower bounds $\boldsymbol{lb}$ (Mathworks, 2017):

$$\min_{\hat{\boldsymbol{z}}} f^T\boldsymbol{x} \text{ such that } \begin{cases} \boldsymbol{Ax} \leq \boldsymbol{b} \\ \boldsymbol{A}_{\boldsymbol{eq}} \cdot \boldsymbol{x} = \boldsymbol{b}_{\boldsymbol{eq}} \\ \boldsymbol{lb} \leq \boldsymbol{x} \end{cases} \tag{A12}$$

Deleted: 11

Deleted: (6)

If the stream network consists of n nodes, $f = [(\tau\ \tau\ ...\ \tau)\quad 1-(\tau\ \tau\ ...\ \tau)\quad (0\ 0\ ...\ 0)]^T$ with n elements concatenated in each vector indicated by the round brackets. $Aeq = [\boldsymbol{I}\quad -\boldsymbol{I}\quad \boldsymbol{I}]$ where $\boldsymbol{I}$ is a nxn identity matrix and $\boldsymbol{beq} = \boldsymbol{z}$. $\boldsymbol{A} = [\boldsymbol{0}\quad \boldsymbol{0}\quad -\boldsymbol{G}]$ with $\boldsymbol{0}$ being a nxn matrix of zeros and $\boldsymbol{G}$ is the gradient matrix introduced in Appendix A1, and $\boldsymbol{b} = [(0\ 0\ ...\ 0)]^T$. The lower bounds are $\boldsymbol{lb} = [(0\ 0\ ...\ 0)\quad (0\ 0\ ...\ 0)\quad -(\infty\ \infty\ ...\ \infty)]^T$. The linear program returns the vector $\boldsymbol{x}$ whose elements $2n+1$ to $3n$ refer to the elevation values $\hat{\boldsymbol{z}}$.

A4 CRS algorithm

Equation 3 is solved by quadratic programming. A quadratic programming problem has an objective which is a quadratic function of the variables in x:

$$\min_{\hat{\boldsymbol{z}}} \frac{1}{2}\boldsymbol{x^T H x} + \boldsymbol{f^T x} \text{ such that } \begin{cases} \boldsymbol{Ax \le b} \\ \boldsymbol{A_{eq} \cdot x = b_{eq}} \\ \boldsymbol{lb \le x} \end{cases} \tag{A13}$$

where the notation is the same as in Appendix A3. The quadratic term in the problem is

$$\boldsymbol{H} = \begin{bmatrix} \boldsymbol{0} & \boldsymbol{0} & \boldsymbol{0} \\ \boldsymbol{0} & \boldsymbol{0} & \boldsymbol{0} \\ \boldsymbol{0} & \boldsymbol{0} & \boldsymbol{B} \end{bmatrix} \tag{A14}$$

where $\boldsymbol{0}$ being a nxn matrix of zeros and $\boldsymbol{B} = 2(\boldsymbol{D^T D})$ and

$$D = \begin{bmatrix} \boldsymbol{0} \\ s\boldsymbol{C} \end{bmatrix} \tag{A15}$$

where s determines the smoothness of the profile (Eq. A7) and $\boldsymbol{C}$ is second order finite difference matrix introduced in Appendix A1. The quadratic program returns the vector $\boldsymbol{x}$ whose elements $2n+1$ to $3n$ refer to the elevation values $\hat{\boldsymbol{z}}$.

Appendix B

Appendix B1: Software implementation and code availability

A software implementation of the CRS algorithm is available for the MATLAB software TopoToolbox on https://github.com/wschwanghart/topotoolbox. The software allows tuning several parameters. The parameter K dictates the degree of smoothing. The choice of the value of K involves a tradeoff between filtering river-profile variability present in reality and retaining data artifacts. Too high values of K may introduce new artifacts. Estimating a suitable value of K depends on both the type and magnitudes of errors in the data and the type of applications. Benchmark data such as LiDAR

DEMs and precise (differential) global positioning system measurements can be used to estimate optimal parameter values that provide the best fit between the benchmark data and the DEM. If benchmark data is unavailable, visual crosschecking the results of the algorithm with variable parameters can guide the choice of suitable parameter settings. We developed a graphical user interface in TopoToolbox (*crsapp*) that supports a trial-and-error approach and visual crosschecking. Additional examples and applications of the algorithms can be found on http://topotoolbox.wordpress.com.

References

Ahuja, R. K., Magnanti, T. L. and Orlin, J. B.: Network flows: theory, algorithms, and applications, Prentice Hall., 1993.

Aiken, S. J. and Brierley, G. J.: Analysis of longitudinal profiles along the eastern margin of the Qinghai-Tibetan Plateau, J. Mt. Sci., 10(4), 643–657, doi:10.1007/s11629-013-2814-2, 2013.

Baade, J. and Schmullius, C.: Uncertainties of a TanDEM-X derived Digital Surface Model: A case study from the Roda catchment, Germany, in Geoscience and Remote Sensing Symposium (IGARSS), 2014 IEEE International, pp. 4327–4330., 2014.

Bishop, P., Hoey, T. B., Jansen, J. D. and Artza, I. L.: Knickpoint recession rate and catchment area: the case of uplifted rivers in Eastern Scotland, Earth Surf. Process. Landf., 30(6), 767–778, doi:10.1002/esp.1191, 2005.

Brardinoni, F. and Hassan, M. A.: Glacial erosion, evolution of river long profiles, and the organization of process domains in mountain drainage basins of coastal British Columbia, Journal of Geophysical Research, 111, F01013–F01013, 2006.

Bricker, J. D., Schwanghart, W., Adhikari, B. R., Moriguchi, S., Roeber, V. and Giri, S.: Performance of Models for Flash Flood Warning and Hazard Assessment: The 2015 Kali Gandaki Landslide Dam Breach in Nepal, Mt. Res. Dev., 37(1), 5–15, doi:10.1659/MRD-JOURNAL-D-16-00043.1, 2017.

Canters, F., Genst, W. D. and Dufourmont, H.: Assessing effects of input uncertainty in structural landscape classification, Int. J. Geogr. Inf. Sci., 16(2), 129–149, doi:10.1080/13658810110099143, 2002.

Carlisle, B. H.: Modelling the spatial distribution of DEM error, Trans. GIS, 9(4), 521–540, doi:10.1111/j.1467-9671.2005.00233.x, 2005.

Czubski, K., Kozak, J. and Kolecka, N.: Accuracy of SRTM-X and ASTER elevation data and its influence on topographical and hydrological modeling; Case study of the Pieniny Mts. in Poland, Int. J. Geoinformatics, 9(2), 2013.

De Smith, M.J., Goodchild, M.F., Longley, P. (2007): Geospatial analysis: a comprehensive guide to principles, techniques and software tools. Troubador.

Devrani, R., Singh, V., Mudd, S. M. and Sinclair, H. D.: Prediction of flash flood hazard impact from Himalayan river profiles, Geophys. Res. Lett., 42(14), 2015GL063784, doi:10.1002/2015GL063784, 2015.

Falorni, G., Teles, V., Vivoni, E. R., Bras, R. L. and Amaratunga, K. S.: Analysis and characterization of the vertical accuracy of digital elevation models from the Shuttle Radar Topography Mission, J. Geophys. Res. Earth Surf., 110(F2), F02005, doi:10.1029/2003JF000113, 2005.

Deleted: Spatial Distribution
Deleted: Error
Deleted: Elevation Data
Deleted: Influence
Deleted: Topographical
Deleted: Hydrological Modeling
Deleted: Study

Fisher, P. F. and Tate, N. J.: Causes and consequences of error in digital elevation models, Prog. Phys. Geogr., 30(4), 467–489, doi:10.1191/0309133306pp492ra, 2006.

Garcia, D.: Robust smoothing of gridded data in one and higher dimensions with missing values, Comput. Stat. Data Anal., 54(4), 1167–1178, doi:10.1016/j.csda.2009.09.020, 2010.

Gesch, D., Oimoen, M., Zhang, Z., Meyer, D. and Danielson, J.: Validation of the aster global digital elevation model version 2 over the conterminous United States., Int. Arch. Photogramm. Remote Sens. Spat. Inf. Sci., 34(B4), 281–286, 2012.

Gonga-Saholiariliva, N., Gunnell, Y., Harbor, D. and Mering, C.: An automated method for producing synoptic regional maps of river gradient variation: Procedure, accuracy tests, and comparison with other knickpoint mapping methods, Geomorphology, 134(3–4), 394–407, doi:10.1016/j.geomorph.2011.07.013, 2011.

Gorokhovich, Y. and Voustianiouk, A.: Accuracy assessment of the processed SRTM-based elevation data by CGIAR using field data from USA and Thailand and its relation to the terrain characteristics, Remote Sens. Environ., 104(4), 409–415, doi:10.1016/j.rse.2006.05.012, 2006.

Green, P. J., Silverman, B. W. and Silverman, B. W.: Nonparametric Regression and Generalized Linear Models: A Roughness Penalty Approach, Chapman & Hall, London ; New York., 1993.

Gruber, A., Wessel, B., Huber, M. and Roth, A.: Operational TanDEM-X DEM calibration and first validation results, ISPRS J. Photogramm. Remote Sens., 73, 39–49, doi:10.1016/j.isprsjprs.2012.06.002, 2012a.

Gruber, A., Wessel, B., Huber, M., Breunig, M., Wagenbrenner, S. and Roth, A.: Quality assessment of first TanDEM-X DEMs for different terrain types, in EUSAR 2012; 9th European Conference on Synthetic Aperture Radar, pp. 101–104., 2012b.

Guth, P. L.: Contour line “ghosts” in USGS Level 2 DEMs, Photogramm. Eng. Remote Sens., 65(3), 289–296, 1999.

Guth, P. L.: Geomorphometry from SRTM: Comparison to NED, Photogramm. Eng. Remote Sens., 72, 269–277, 2006.

Hack, J. T.: Studies of longitudinal stream profiles in Virginia and Maryland, USGS Prof. Pap., 295, 45-97, 1957.

Hancock, G. R., Martinez, C., Evans, K. G. and Moliere, D. R.: A comparison of SRTM and high-resolution digital elevation models and their use in catchment geomorphology and hydrology: Australian examples, Earth Surf. Process. Landf., 31, 1394–1412, 2006.

Harbor, D., Bacastow, A., Heath, A. and Rogers, J.: Capturing variable knickpoint retreat in the central Appalachians, USA, Geografia Fisica e Dinamica Quaternaria, 28, 23–36, 2005.

Hayakawa, Y. S. and Oguchi, T.: DEM-based identification of fluvial knickzones and its application to Japanese mountain rivers, Geomorphology, 78(1–2), 90–106, doi:10.1016/j.geomorph.2006.01.018, 2006.

Hayakawa, Y. S., Oguchi, T. and Lin, Z.: Comparison of new and existing global digital elevation models: ASTER G-DEM and SRTM-3, Geophys. Res. Lett., 35(17), L17404, doi:10.1029/2008GL035036, 2008.

Heckmann, T., Schwanghart, W. and Phillips, J. D.: Graph theory—Recent developments of its application in geomorphology, Geomorphology, 243, 130–146, doi:10.1016/j.geomorph.2014.12.024, 2015.

Hengl, T.: Finding the right pixel size, Comput. Geosci., 32(9), 1283–1298, doi:10.1016/j.cageo.2005.11.008, 2006.

Holmes, K. W., Chadwick, O. A. and Kyriakidis, P. C.: Error in a USGS 30-meter digital elevation model and its impact on terrain modeling, J. Hydrol., 233(1–4), 154–173, doi:10.1016/S0022-1694(00)00229-8, 2000.

Howard, A. D.: Long Profile Development of Bedrock Channels: Interaction of Weathering, Mass Wasting, Bed Erosion, and Sediment Transport, in Rivers Over Rock: Fluvial Processes in Bedrock Channels, edited by K. J. Tinkler and E. E. Wohl, pp. 297–319, American Geophysical Union, 1998.

Hutchinson, M. F., Xu, T. and Stein, J. A.: Recent progress in the ANUDEM elevation gridding procedure, pp. 19–22, Redlands, CA., 2011.

James, M. R. and Robson, S.: Mitigating systematic error in topographic models derived from UAV and ground-based image networks, Earth Surf. Process. Landf., 39(10), 1413–1420, doi:10.1002/esp.3609, 2014.

Jarihani, A. A., Callow, J. N., McVicar, T. R., Van Niel, T. G. and Larsen, J. R.: Satellite-derived Digital Elevation Model (DEM) selection, preparation and correction for hydrodynamic modelling in large, low-gradient and data-sparse catchments, J. Hydrol., 524, 489–506, doi:10.1016/j.jhydrol.2015.02.049, 2015.

Jarvis, A., Reuter, H. I., Nelson, A. and Guevara, E.: Hole-filled seamless SRTM data V4, 2008.

Koenker, R.: Quantile Regression, Cambridge University Press, Cambridge ; New York., 2010.

Korup, O.: Rock-slope failure and the river long profile, Geology, 34(1), 45–48, doi:10.1130/G21959.1, 2006.

Lindsay, J. B.: Efficient hybrid breaching-filling sink removal methods for flow path enforcement in digital elevation models, Hydrol. Process., 846–857, doi:10.1002/hyp.10648, 2016.

Lindsay, J. B. and Dhun, K.: Modelling surface drainage patterns in altered landscapes using LiDAR, Int. J. Geogr. Inf. Sci., 29(3), 397–411, doi:10.1080/13658816.2014.975715, 2015.

Ludwig, R. and Schneider, P.: Validation of digital elevation models from SRTM X-SAR for applications in hydrologic modeling, ISPRS J. Photogramm. Remote Sens., 60(5), 339–358, doi:10.1016/j.isprsjprs.2006.05.003, 2006.

Malinowski, R., Höfle, B., Koenig, K., Groom, G., Schwanghart, W. and Heckrath, G.: Local-scale flood mapping on vegetated floodplains from radiometrically calibrated airborne LiDAR data, ISPRS J. Photogramm. Remote Sens., 119, 267–279, doi:10.1016/j.isprsjprs.2016.06.009, 2016.

Mathworks: MATLAB Documentation (R2017a), 2017.

McMaster, K. J.: Effects of digital elevation model resolution on derived stream network positions, Water Resour. Res., 38(4), 13–1, doi:10.1029/2000WR000150, 2002.

Mudd, S. M., Attal, M., Milodowski, D. T., Grieve, S. W. D. and Valters, D. A.: A statistical framework to quantify spatial variation in channel gradients using the integral method of channel profile analysis, J. Geophys. Res. Earth Surf., 119(2), 2013JF002981, doi:10.1002/2013JF002981, 2014.

Nardi, F., Grimaldi, S., Santini, M., Petroselli, A. and Ubertini, L.: Hydrogeomorphic properties of simulated drainage patterns using digital elevation models: the flat area issue / Propriétés hydro-géomorphologiques de réseaux de drainage

simulés à partir de modèles numériques de terrain: la question des zones planes, Hydrol. Sci. J., 53(6), 1176–1193, doi:10.1623/hysj.53.6.1176, 2008.

Neely, A. B., Bookhagen, B. and Burbank, D. W.: An automated knickzone selection algorithm (KZ-Picker) to analyze transient landscapes: Calibration and validation, J. Geophys. Res. Earth Surf., 2017JF004250, doi:10.1002/2017JF004250, 2017.

O'Callaghan, J. F. and Mark, D. M.: The extraction of drainage networks from digital elevation data, Comput. Vis. Graph. Image Process., 28(3), 323–344, doi:10.1016/S0734-189X(84)80011-0, 1984.

Oksanen, J. and Sarjakoski, T.: Uncovering the statistical and spatial characteristics of fine toposcale DEM error, Int. J. Geogr. Inf. Sci., 20(4), 345–369, doi:10.1080/13658810500433891, 2006.

Opsomer, J., Wang, Y. and Yang, Y.: Nonparametric Regression with Correlated Errors, Statistical Science, 16(2), 134–153, 2001.

Paiva, R. C. D., Collischonn, W. and Tucci, C. E. M.: Large scale hydrologic and hydrodynamic modeling using limited data and a GIS based approach, J. Hydrol., 406(3–4), 170–181, doi:10.1016/j.jhydrol.2011.06.007, 2011.

Purinton, B. and Bookhagen, B.: Validation of digital elevation models (DEMs) and comparison of geomorphic metrics on the southern Central Andean Plateau, Earth Surf. Dyn., 5(2), 211–237, doi:10.5194/esurf-5-211-2017, 2017.

Rabus, B., Eineder, M., Roth, A. and Bamler, R.: The shuttle radar topography mission—a new class of digital elevation models acquired by spaceborne radar, ISPRS J. Photogramm. Remote Sens., 57(4), 241–262, doi:10.1016/S0924-2716(02)00124-7, 2003.

Reuter, H. I., Hengl, T., Gessler, P. and Soille, P.: Preparation of DEMs for geomorphometric analysis, in Geomorphometry. Concepts, Software, Applications, vol. 33, edited by T. Hengl and H. I. Reuter, pp. 87–120, Elsevier., 2009.

Rizzoli, P., Bräutigam, B., Kraus, T., Martone, M. and Krieger, G.: Relative height error analysis of TanDEM-X elevation data, ISPRS J. Photogramm. Remote Sens., 73, 30–38, doi:10.1016/j.isprsjprs.2012.06.004, 2012.

Scherler, D., Bookhagen, B. and Strecker, M. R.: Tectonic control on 10Be-derived erosion rates in the Garhwal Himalaya, India, Journal of Geophysical Research: Earth Surface, n/a–n/a, doi:10.1002/2013JF002955, 2014.

Scherler, D., Leprince, S. and Strecker, M. R.: Glacier-surface velocities in alpine terrain from optical satellite imagery—Accuracy improvement and quality assessment, Remote Sens. Environ., 112(10), 3806–3819, doi:10.1016/j.rse.2008.05.018, 2008.

Schwanghart, W. and Heckmann, T.: Fuzzy delineation of drainage basins through probabilistic interpretation of diverging flow algorithms, Environ. Model. Softw., 33, 106–113, doi:10.1016/j.envsoft.2012.01.016, 2012.

Schwanghart, W. and Scherler, D.: TopoToolbox 2 – MATLAB-based software for topographic analysis and modeling in Earth surface sciences, Earth Surf. Dyn., 2, 1–7, doi:10.5194/esurf-2-1-2014, 2014.

Schwanghart, W., Groom, G., Kuhn, N. J. and Heckrath, G.: Flow network derivation from a high resolution DEM in a low relief, agrarian landscape, Earth Surf. Process. Landf., 38, 1576–1586, 2013.

Shepherd, R. G.: Regression Analysis of River Profiles, J. Geol., 93(3), 377–384, 1985.

Sivia, D. S. and Skilling, J.: Data analysis. A Bayesian Tutorial, 2nd ed., Oxford University Press, Oxford, New York., 2006.

Sofia, G., Fontana, G. D. and Tarolli, P.: High-resolution topography and anthropogenic feature extraction: testing geomorphometric parameters in floodplains, Hydrol. Process., 28, 2046-2061, doi:10.1002/hyp.9727, 2013.

Soille, P.: Optimal removal of spurious pits in grid digital elevation models, Water Resour. Res., 40(12), W12509, doi:10.1029/2004WR003060, 2004.

Soille, P., Vogt, J. and Colombo, R.: Carving and adaptive drainage enforcement of grid digital elevation models, Water Resour. Res., 39, SWC-10.1-13, doi:10.1029/2002WR001879, 2003.

Tachikawa, T., Hato, M., Kaku, M. and Iwasaki, A.: Characteristics of ASTER GDEM version 2, in Geoscience and Remote Sensing Symposium (IGARSS), 2011 IEEE International, pp. 3657–3660., 2011.

Takaku, J., Tadono, T. and Tsutsui, K.: Generation of High Resolution Global DSM from ALOS PRISM, ISPRS - Int. Arch. Photogramm. Remote Sens. Spat. Inf. Sci., XL-4, 243–248, doi:10.5194/isprsarchives-XL-4-243-2014, 2014.

Takeuchi, I., Quoc, V. L., Sears, T. and Smola, A. J.: Nonparametric quantile regression, J. Mach. Learn. Res., 7, 1001–1032, 2005.

Temme, A. J. A. ., Heuvelink, G. B. M., Schoorl, J. M. and Claessens, L.: Geostatistical simulation and error propagation in geomorphometry, in Geomorphometry. Concepts, Software, Applications, vol. 33, edited by T. Hengl and H. I. Reuter, pp. 121–140, Elsevier., 2009.

Vaze, J., Teng, J. and Spencer, G.: Impact of DEM accuracy and resolution on topographic indices, Environmental Modelling & Software, 25(10), 1086–1098, doi:10.1016/j.envsoft.2010.03.014, 2010.

Watson, C. S., Carrivick, J. and Quincey, D.: An improved method to represent DEM uncertainty in glacial lake outburst flood propagation using stochastic simulations, J. Hydrol., 529, Part 3, 1373–1389, doi:10.1016/j.jhydrol.2015.08.046, 2015.

Wechsler, S. P. and Kroll, C. N.: Quantifying DEM Uncertainty and its Effect on Topographic Parameters, Photogramm. Eng. Remote Sens., 72(9), 1081–1090, doi:10.14358/PERS.72.9.1081, 2006.

Wessel, B.: TanDEM-X ground segment DEM product specification document, DLR, TD-GS-PS-0021, 2016.

Whipple, K. X., DiBiase, R. A. and Crosby, B. T.: Bedrock Rivers, in Treatise on Geomorphology, pp. 550–573, Elsevier, 2013.

Wobus, C., Whipple, K. X., Kirby, E., Snyder, N., Johnson, J., Spyropolou, K., Crosby, B. and Sheehan, D.: Tectonics from topography: procedures, promise, and pitfalls, GSA Spec. Pap., 398, 55–74, doi:10.1130/2006.2398(04), 2006.

Tables

Table 1: Digital elevation models (DEM) used in this study.

	Yakima River, Central Washington	Big Tujunga, California	Kali Gandaki, Central Nepal
Benchmark DEM	Airborne LiDAR[1]	Airborne LiDAR[1]	-
DEMs	AW3D[3], ASTER GDEM[4], SRTM1[5]	AW3D[3], ASTER GDEM[4], SRTM1[5]	TanDEM-X DEM2, AW3D[3], ASTER GDEM[4], SRTM1[5]
Coordinates	46.83°N, 120.46°W	34.17°N, 118.16°W	28.16°N, 83.80°E
Topographic range (min, max)	630 m (360 – 990 m a.s.l.)	2000 m (300 – 2300 m a.s.l.)	8050 m (50 – 8100 m a.s.l.)

[1] Bare earth DEMs from the National Center for Airborne Laser Mapping; spatial resolution of 0.5 m; elevation accuracy 5-30 cm typical (±1-sigma); downloaded from http://www.opentopography.org

[2] Derived from X-band interferometric synthetic aperture radar data; spatial resolution of 12 m; absolute vertical accuracy <10 m (linear error at 90% confidence level); acquired, produced and provided by DLR (Wessel, 2016)

[3] ALOS World 3D 30; derived from ALOS PRISM stereo images; spatial resolution of 30 m; vertical error 5 m (root mean squared error); released by the Japan Aerospace Exploration Agency (JAXA) (Takaku et al., 2014) and downloaded from http://www.opentopography.org

[4] Version 2; spatial resolution of 30 m; ASTER GDEM is a product of NASA and METI; vertical accuracy 13 m (±1-sigma) (Tachikawa et al., 2011); downloaded from http://lpdaac.usgs.gov

[5] Shuttle Radar Topography Mission (Jarvis et al., 2008); spatial resolution of 30 m; absolute vertical accuracy <16 m (Falorni et al., 2005); downloaded from http://www.opentopography.org

Deleted: ,

Table 2: Statistics of offsets between river-profile elevations derived from different global DEMs and benchmark LiDAR DEMs. τ_0 refers to the quantile of the profile data where the offset between LiDAR and global DEMs is zero.

		SRTM-1	AW3D	ASTER GDEM
Yakima	Mean (bias) [m]	3.61	0.19	2.16
(low relief)	Standard deviation [m]	2.95	3.03	7.34
	Skewness	0.46	3.95	-0.61
	τ_0	0.11	0.55	0.37
Big Tujunga	Mean (bias) [m]	15.93	5.90	10.08
(medium relief)	Standard deviation [m]	8.11	4.98	8.23
	Skewness	0.94	1.76	0.52
	τ_0	0.01	0.03	0.10

Table 3: Statistical characterisation of residuals from smoothed river profiles derived with the CRS algorithm (K=5, τ=0.5) from globally available DEMs and at different sites.

	DEM	Residual mean [m]	RMSE [m]	Minimum [m]	Maximum [m]	Skewness	Kurtosis
Yakima	SRTM-1	-0.15	2.05	-21.19	9.89	-2.52	21.03
(low relief)	AW3D	-0.17	1.78	-19.00	7.77	-3.61	32.96
	ASTER GDEM	-0.23	4.51	-37.00	17.12	-1.28	11.85
Big Tujunga	SRTM-1	0.05	3.40	-27.60	23.59	0.14	12.28
(medium relief)	AW3D	0.16	2.97	-34.44	38.83	0.90	29.03
	ASTER GDEM	-0.06	3.89	-29.85	28.93	-0.20	8.54
Kali Gandaki	SRTM-1	0.71	7.24	-39.75	106.73	4.45	45.81
(high relief)	AW3D	0.05	1.97	-12.20	40.98	4.96	72.61
	ASTER GDEM	0.48	15.20	-78.99	114.22	0.56	8.86
	TanDEM-X DEM	1.19	18.79	-236.84	172.84	2.36	27.41

Table 4: Optimal values of K and τ for CRS algorithm applied to the Yakima and Big Tujunga catchments and different DEMs. **The root mean squared error (RMSE) is calculated from the deviations from the LiDAR data.**

	DEM	K	τ	RMSE [m]	RMSE with CRS [m]	RMSE with carving [m]	RMSE with filling [m]
Yakima	SRTM-1	2.76	0.05	4.66	2.57	3.90	6.78
(low relief)	AW3D	0.53	0.40	3.04	1.48	5.61	14.40
	ASTER GDEM	21.93	0.37	7.65	3.86	12.71	13.73
Big Tujunga	SRTM-1	1.57	0.01	17.88	11.68	16.16	20.33
(medium relief)	AW3D	1.00	0.06	7.72	5.41	7.01	10.01
	ASTER GDEM	2.57	0.03	13.01	7.92	11.77	14.37

Figures

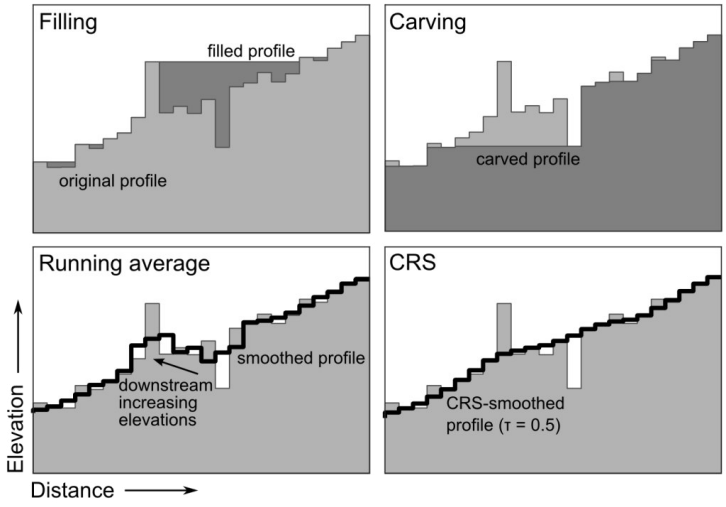

Fig. 1: Detail of a longitudinal river profile and effects of different techniques to hydrologically correct and smooth the profile.

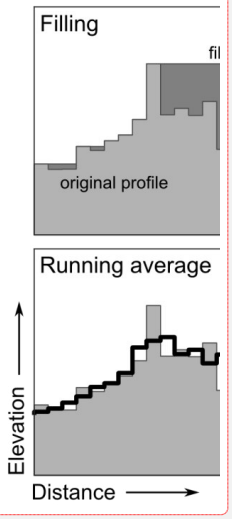

Deleted:

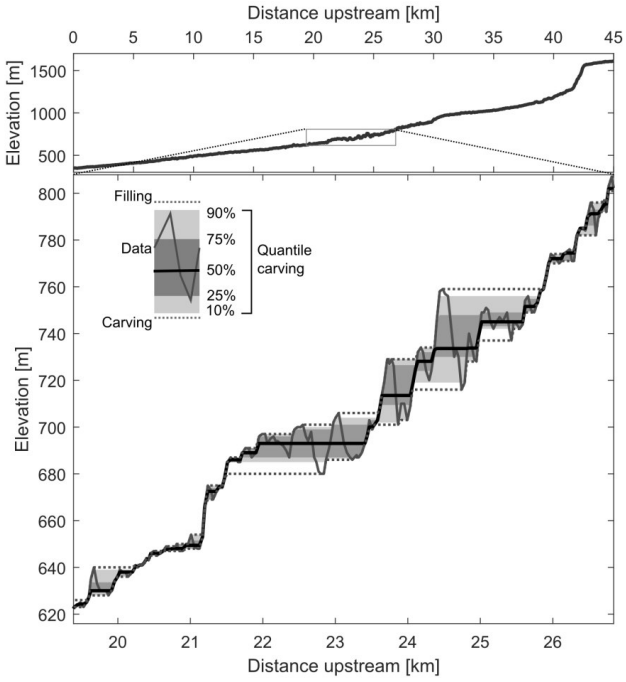

Fig. 2: Quantile carving of the longitudinal profile of the Big Tujunga river. Quantile carving reconstructs the profile along different quantiles and thus continuously links the two common approaches carving and filling that run along minima and maxima of the data, respectively.

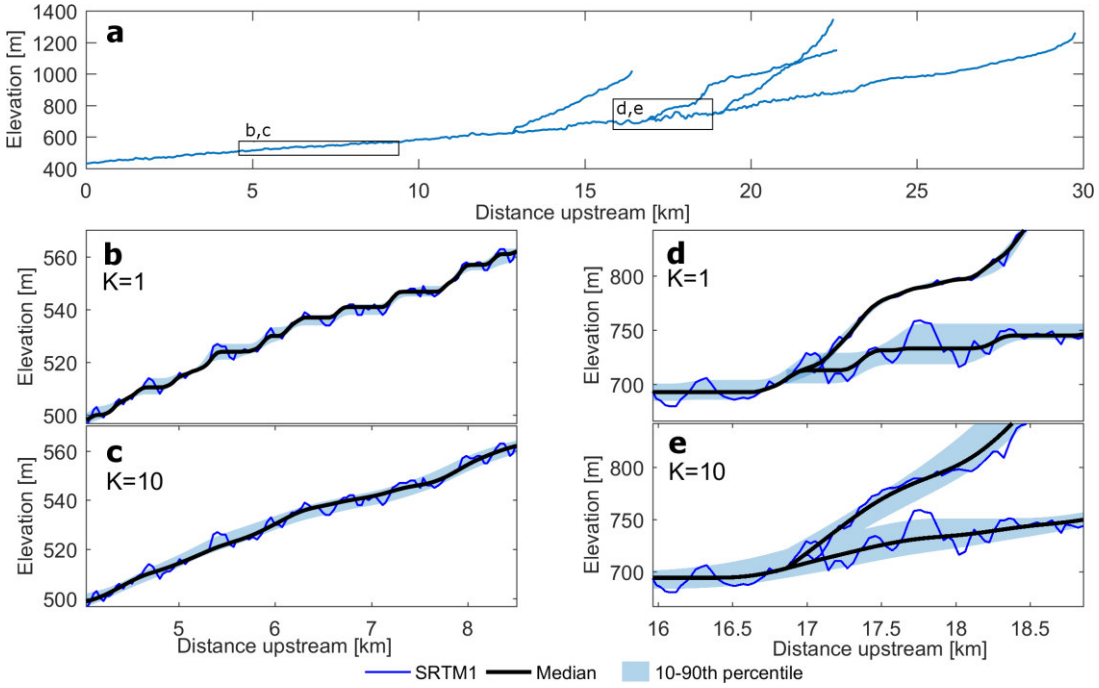

Fig. 3: Applying the CRS-algorithm to selected streams in the Big Tujunga catchment (a). Panels b-e show details of the longitudinal river profile and results for the median and 10-90th percentile for the smoothing parameter *K*=1 and *K*=10.

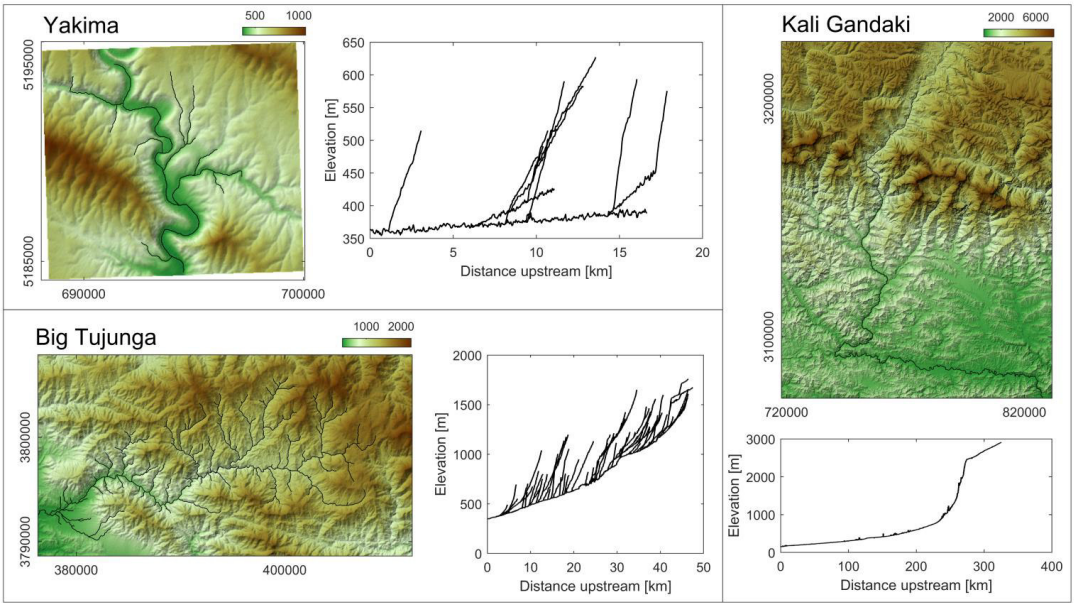

Fig. 4: Sites and longitudinal river profiles in this study. Shaded reliefs are derived from SRTM-1 and colours indicate elevation in meters.

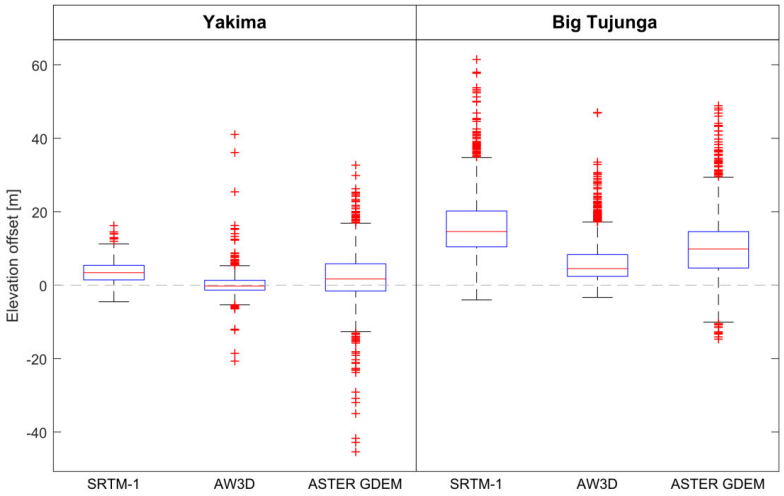

Fig. 5: Elevation offsets between different DEMs and benchmark LiDAR DEMs calculated for all river pixels for the Yakima and Big Tujunga dataset (see Fig. 4).

Deleted: Offsets of river elevations

Deleted: .

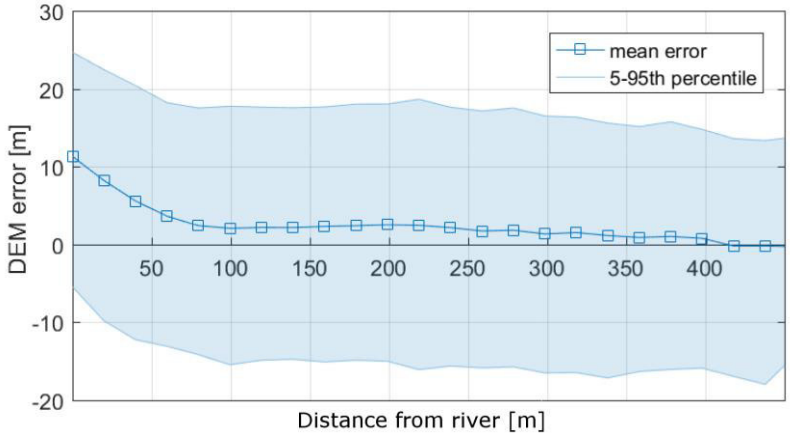

Fig. 6: Bias of the SRTM-1 in the Big Tujunga catchment approaches zero with increasing distance from the river.

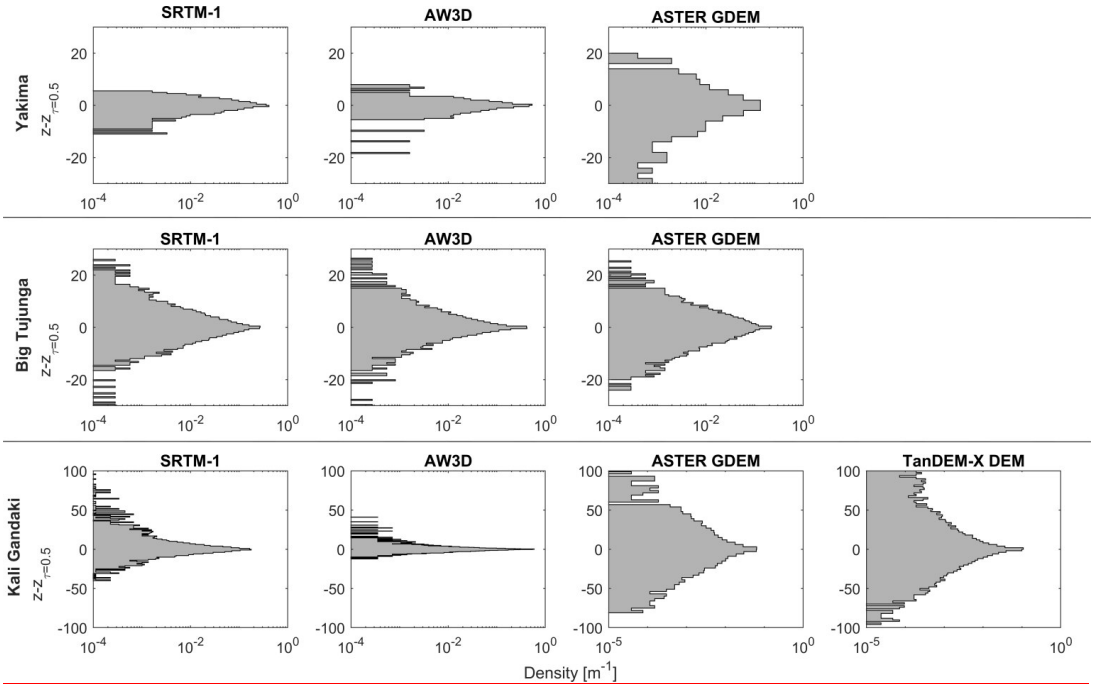

Fig. 7: Error distributions of longitudinal river profiles along theYakima, Big Tujunga and Kali Gandaki calculated by the offset between measured elevations and elevations obtained with the CRS-algorithm with $\tau = 0.5$ and $K = 5$.

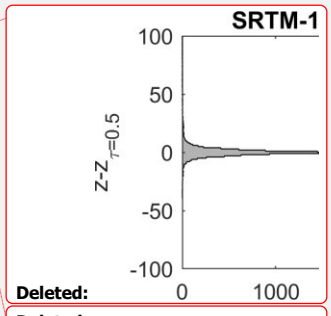

Deleted:

Deleted: the

Deleted: heights

Deleted: heights

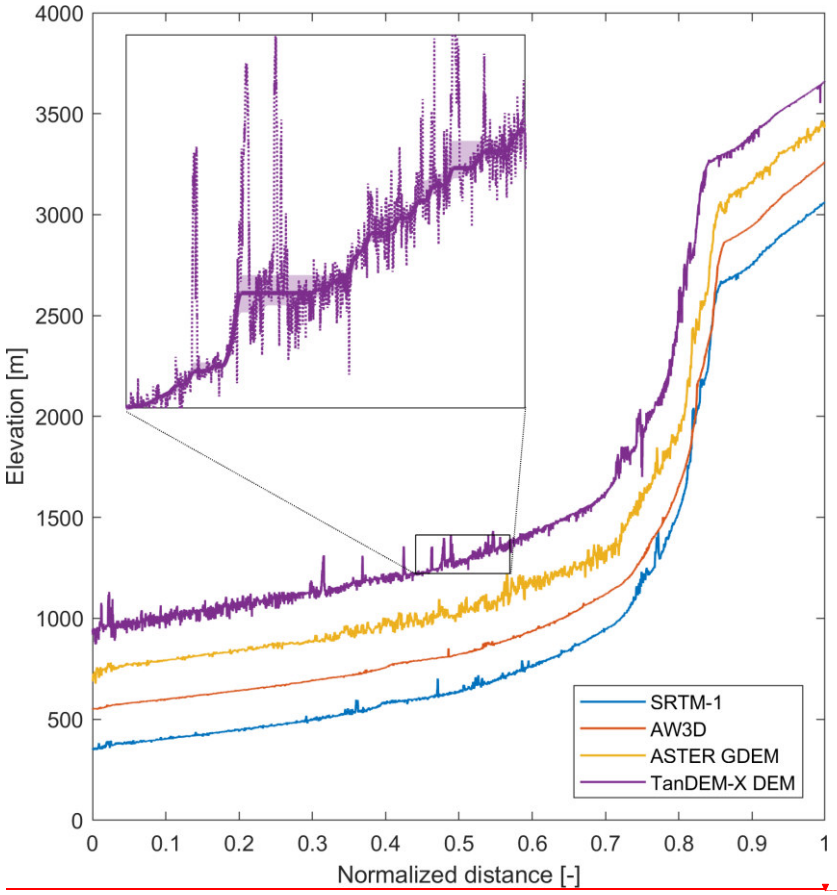

Deleted: ¶
¶

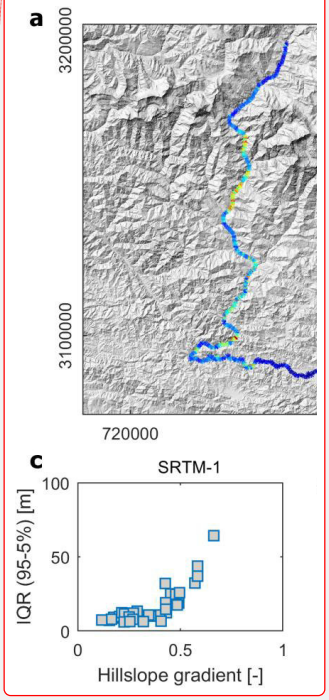

Fig. 8: Profiles derived from different global DEMs for the Kali Gandaki, Nepal. Horizontal distances along rivers vary and were thus normalized to range between 0 and 1. The inset shows details from the TanDEM-X DEM derived profile where the dashed line is the original data, the solid is the CRS-derived profile (K=10, τ = 0.5) and the shaded area delineates the interquartile range derived with the CRS algorithm (K=10, τ = 0.25 and 0.75).

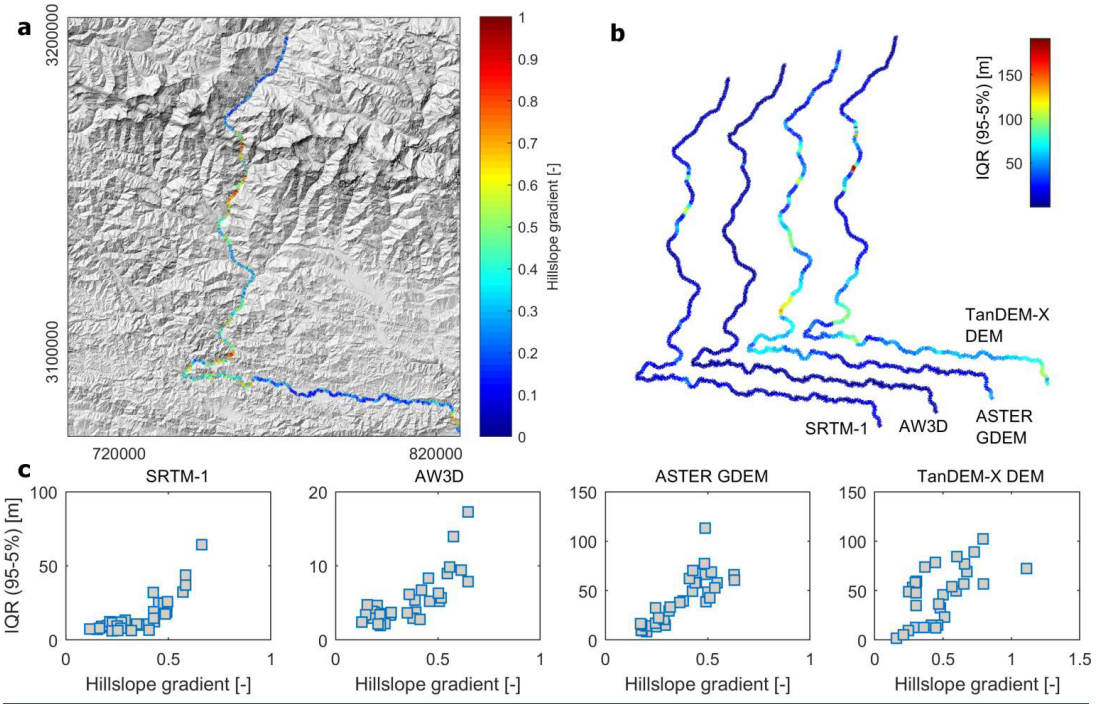

Fig. 9: Planform patterns of DEM errors along the Kali Gandaki (a, b). The interquantile range (IQR) correlates with hillslope gradients adjacent to river (within <1000 m distance) (c).

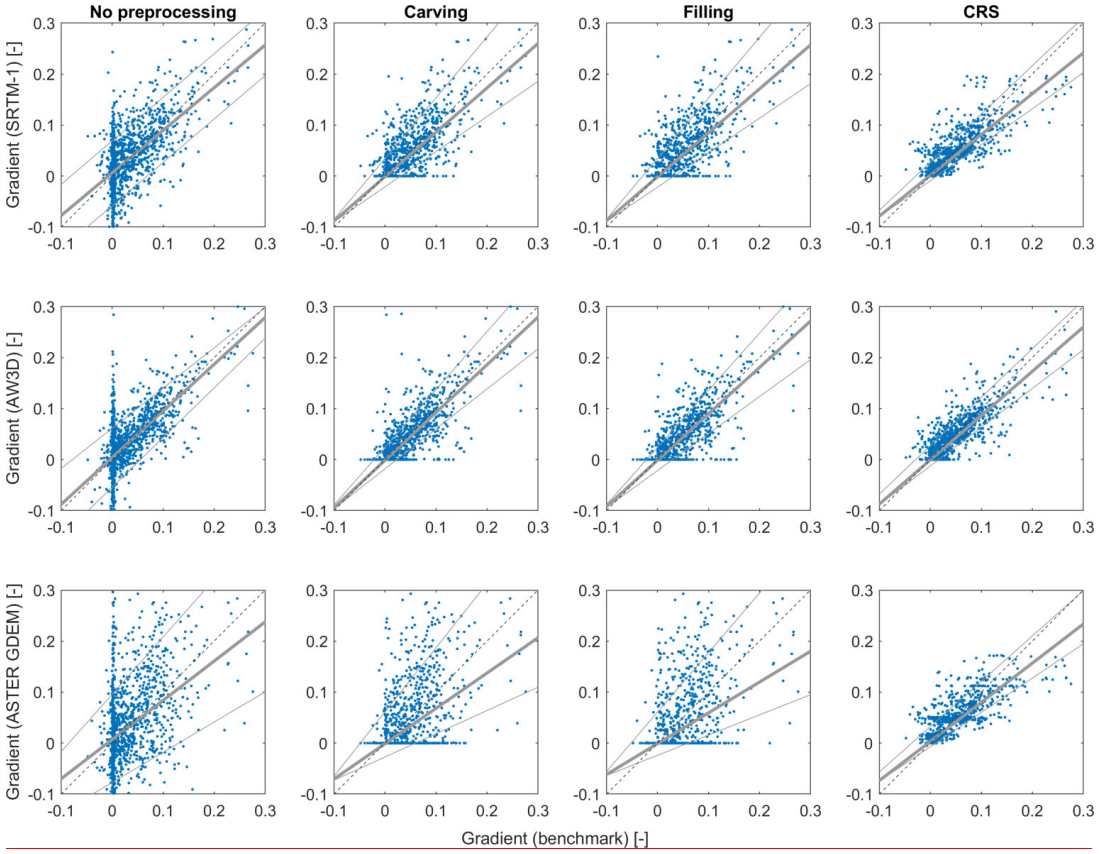

Fig. 10: Comparison of pixel-by-pixel along-river gradients derived from benchmark LiDAR DEMs (resampled to 30 m) and global DEMs in the Yakima catchment. Negative gradients in the benchmark and unprocessed DEMs are due to erroneously increasing river elevations in downstream direction. The grey solid lines (thin lines: 10 and 90%iles, thick line: median) are derived from a quantile regression. The dashed line is a one-to-one reference line. The parameters of the CRS algorithm (τ and K) are those in Table 4 of the manuscript. Compared to the original profiles and those obtained by preprocessing techniques filling and carving, the CRS algorithm is able to reduce the differences between along-river gradients as indicated by the narrow interquantile (90-10%iles) range.

Deleted: Page Break

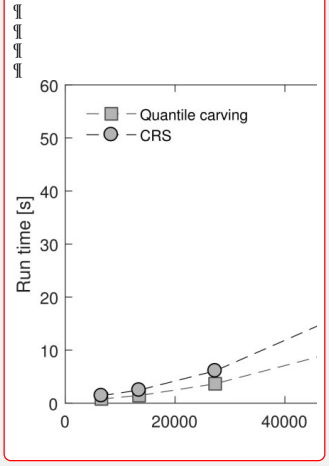

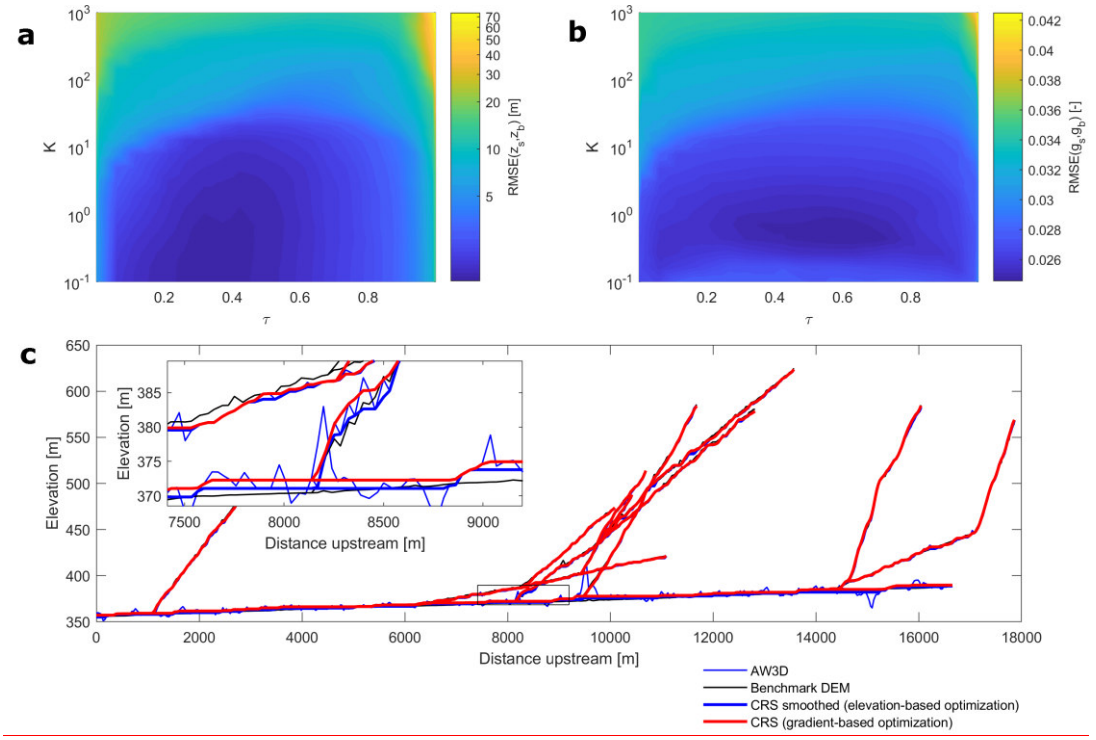

Fig. 11: Sensitivity analysis of the CRS algorithm and the smoothing parameter K and quantile τ for the Yakima catchment and the AW3D DEM. a) Sensitivity of the root mean squared error (RMSE) between smoothed elevations and elevations from the LiDAR derived benchmark profile. b) Sensitivity of the RMSE between gradients derived from the smoothed profiles and the benchmark profile. c) Profile of the Yakima and its tributaries and detail (see inset).

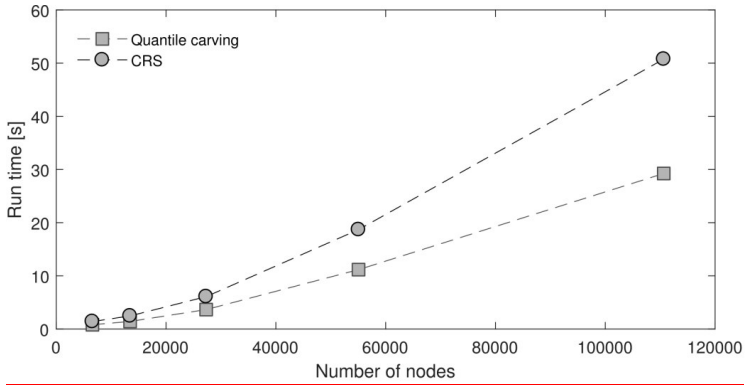

Fig. 12: Run time of quantile carving and the CRS algorithm for river networks with different sizes. The number of nodes refers to the pixels in the DEM that constitute river pixels. Tests were run on a Windows 7 system with an Intel Xeon CPU (3.07 GHz, 4 cores) and 24 GB installed memory (RAM).